

FAUST – XXII. Deuteration in the VLA1623-2417 protostellar hot-corinos, cavities, and streamers.

S. Mercimek,^{1,2*} C. Codella^{2,3}, L. Podio², P. Caselli⁴, C. J. Chandler⁵, L. Chahine³, S. Ohashi⁶, G. Sabatini², L. Loinard^{7,8}, D. Johnstone^{9,10}, E. Bianchi², Y. Zhang¹¹, M. De Simone¹², C. Ceccarelli³, N. Sakai⁶, S. Yamamoto¹³

¹ *Jodrell Bank Centre for Astrophysics, UK ALMA Regional Centre Node, University of Manchester, Manchester M13 9PL, UK*

² *INAF, Osservatorio Astrofisico di Arcetri, Largo E. Fermi 5, I-50125, Firenze, Italy*

³ *Univ. Grenoble Alpes, CNRS, IPAG, 38000 Grenoble, France*

⁴ *Max-Planck-Institut für extraterrestrische Physik (MPE), Gießenbachstr. 1, D-85741 Garching, Germany*

⁵ *National Radio Astronomy Observatory, PO Box O, Socorro, NM 87801, USA*

⁶ *RIKEN Cluster for Pioneering Research, 2-1, Hirosawa, Wako-shi, Saitama 351-0198, Japan*

⁷ *Instituto de Radioastronomía y Astrofísica, Universidad Nacional Autónoma de México, A.P. 3-72 (Xangari), 8701, Morelia, Mexico*

⁸ *Instituto de Astronomía, Universidad Nacional Autónoma de México, Ciudad Universitaria, A.P. 70-264, Ciudad de México 04510, Mexico*

⁹ *NRC Herzberg Astronomy and Astrophysics, 5071 West Saanich Road, Victoria, BC V9E 2E7, Canada*

¹⁰ *Department of Physics and Astronomy, University of Victoria, Elliott Building, 3800 Finnerty Road, Victoria, BC V8P 5C2, Canada*

¹¹ *Department of Astronomy, University of Virginia, Charlottesville, VA 22904, USA*

¹² *European Southern Observatory, Karl-Schwarzschild-Strasse 2, 85748, Garching bei München, Germany*

¹³ *SOKENDAI (The Graduate University for Advanced Studies), Shonan Village, Hayama, Kanagawa 240-0193, Japan*

Accepted XXX. Received YYY; in original form ZZZ

ABSTRACT

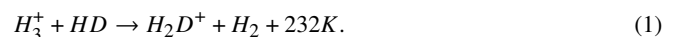
The study of deuterium fractionation is a valuable tool for reconstructing our chemical history from the early prestellar stages to the formation of planets. In the context of the ALMA Large Programme FAUST, we observed formaldehyde, H₂CO, and its singly and doubly deuterated forms, HDCO and D₂CO, towards the protostellar cluster VLA1623–2417, on scales of $\sim 2000 - 50$ au. Formaldehyde probes the inner envelopes of the protostars VLA1623A, B, and W, the rotating cavities opened by the VLA1623A outflow, and several streamers. The HDCO and D₂CO emissions are observed towards VLA1623A, in its outflow cavities, and in one of the streamers. We estimate the gas temperature from the HDCO lines: $T \sim 125$ K towards VLA1623A, indicating hot-corino emission, lower temperatures in the outflow cavities (20 – 40 K), and in the streamers (≤ 15 K). The D₂CO lines also trace the flattened envelope of VLA1623A, where H₂CO and HDCO are fainter. This may be due to D₂CO formation on dust grains in the cold prestellar phase, and subsequent photodesorption caused by the enhanced UV flux from two nearby B stars. We inferred the molecular deuteration: $[\text{HDCO}]/[\text{H}_2\text{CO}] \sim 0.16$, $\sim 0.07 - 0.13$, and ~ 0.3 ; $[\text{D}_2\text{CO}]/[\text{H}_2\text{CO}] \sim 0.003$, $\sim 0.05 - 0.13$, and ~ 0.03 in the hot corino, in the outflow cavities, and in the streamer, respectively. The spatial distribution of D₂CO, which points to formation on dust grains, and the similar values of $[\text{HDCO}]/[\text{H}_2\text{CO}]$ and $[\text{D}_2\text{CO}]/[\text{H}_2\text{CO}]$ in the components of the system, suggest that deuterium fractionation occurs at the prestellar stage and is then inherited, mostly unaltered, in the protostellar phase.

Key words: Stars: formation – Protoplanetary disks – ISM: individual objects: VLA1623–2417

1 INTRODUCTION

Observing how molecular complexity evolves in Sun-like star-forming regions is mandatory to comprehend whether the chemical composition of the protostellar stages is inherited by protoplanetary disks and, possibly, newly formed planets (e.g., Caselli & Ceccarelli 2012). In this context, the deuterium-bearing species are a powerful tool to investigate the chemical evolution along the star formation process (e.g., Ceccarelli et al. 2014, 2023). The deuterium fraction, as observed in the early (prestellar, protostellar) stages of the

star-forming process, can be much larger than the deuterium elemental abundance ($\text{D}/\text{H} \sim 2.5 \times 10^{-5}$, Cooke et al. (2018)). Significant deuteration fraction is seen in the cold (≤ 10 K), dense ($\geq 10^5 \text{ cm}^{-3}$) prestellar cores where most of the species freeze out onto the cold surfaces of the dust grains (e.g., Caselli et al. 2002; Bacmann et al. 2003; Crapsi et al. 2005; Sabatini et al. 2020). When CO is heavily depleted, as in prestellar cores (e.g., Caselli et al. 1999; Bacmann et al. 2002; Sabatini et al. 2022), H₃⁺ can efficiently react with HD via the following exothermic reaction to form its single-deuterated form (e.g., Gerlich et al. 2002; Ceccarelli et al. 2014):



* E-mail: seyma.mercimek@manchester.ac.uk

H_2D^+ can further react with HD to form first D_2H^+ , and then D_3^+ (e.g., Vastel et al. 2004). Once the protostar forms, the accretion of envelope material, the temperature of the protostellar envelope increases, and molecules such as CO and N_2 are released back in the gas phase and react with the deuterated ions, producing an increase in the D/H ratio of several species (Emprechtinger et al. 2009). This applies to both the so-called Class 0 (age $\geq 10^4$ yr), and Class I ($\geq 10^5$ yr) stages (Andre et al. 1990).

Typical examples of species where D/H shows a dramatic enhancement, up to several orders of magnitude, are water, methanol, and formaldehyde (e.g., Loinard et al. 2001; Vastel et al. 2004; Ceccarelli et al. 2007; Caselli & Ceccarelli 2012; Persson et al. 2018; Taquet et al. 2019; Podio et al. 2024; Chahine et al. 2024, and references therein). More specifically, the fractional deuteration of formaldehyde (H_2CO) is an excellent probe to investigate the chemical evolution along the star formation process, being detected from cold prestellar cores (e.g., Chacón-Tanarro et al. 2019) to protoplanetary disks with ages larger than 10^5 yr (e.g., Podio et al. 2024). Formaldehyde can be considered an intermediate species in the process of forming complex organic molecules. It can be formed either in the gas phase or on grains. Gas-phase reactions start with C^+ to form CH_3^+ followed by oxidation (e.g., Roberts & Millar 2000; Turner 2001; Roueff et al. 2007). On the other hand, grain surface formation occurs via multiple hydrogenation of frozen CO (e.g., Tielens 1983; Fuchs et al. 2009; Garrod et al. 2022, and references therein). The deuterated forms of H_2CO are either formed in gas-phase or stored in the grain mantles, where they remain until the protostar is formed and the grain mantles are heated and gradually evaporated (e.g., Ceccarelli et al. 2007).

Gas-phase formaldehyde deuterium fraction has been studied towards low-mass star-forming objects using single-dish antennas (e.g., Bacmann et al. 2003; Parise et al. 2006; Bianchi et al. 2017; Mercimek et al. 2022) and more recently interferometric observations taken in the context of the ALMA programs PILS and FAUST (e.g., Persson et al. 2018; Manigand et al. 2019; Evans et al. 2023; Podio et al. 2024). These observations lead to D/H values $> 10^{-2}$ and $> 10^{-3}$ for HDCO, and D_2CO , respectively. In addition, what has been found so far shows no statistically significant difference in the deuteration fractions in prestellar cores, Class 0 protostars, and Class I/II disks. This suggests that the deuterated molecules in protostars and disks are inherited from the prestellar phase, with little or no reprocessing (Drozdovskaya et al. 2021). However, the available estimates are obtained mainly by using single-dish observations. Therefore, the inferred deuteration is an average over the various structures (hot-corinos, outflows, streamers, envelopes) covered by the beam. Interferometric observations are therefore mandatory to minimise beam dilution and disentangle the inner region (less than 100 au) around protostars from the other physical components such as envelopes, outflows, and infalling streamers.

In this paper, we present observations of formaldehyde and its single- and doubly-deuterated isotopologues toward the prototypical VLA1623–2417 protostellar cluster (Sect. 2). The observations are taken as part of the ALMA Large Program (LP) Fifty AU Study of the chemistry in the disk/envelope system of Solar-like protostars (FAUST, <http://faust-almal.riken.jp>, PI: S. Yamamoto; Codella et al. 2021) (Sect. 3). We analyse the spatial distribution of H_2CO , HDCO, and D_2CO from scales of ~ 2000 au down to scales of 50 au (Sect. 4). We then estimate the gas temperature and the molecular column densities and deuteration towards the detected emission components, i.e. the VLA1623 A hot-corino, the outflow cavities, and the accretion streamers (Sect. 5.1). Finally we discuss the formation mechanism of deuterated molecules and compare our estimates of deuteration in

the different components of VLA1623 with values from the literature (Sects. 5.2 and 5.3). We summarize our conclusions in Sect. 6.

2 THE VLA1623-2417 PROTOSTELLAR CLUSTER

VLA1623-2417 (hereafter VLA1623) is a protostellar cluster located in Ophiuchus A at a distance of 131 ± 1 pc (Gagné et al. 2018). The multiple system has been studied at different wavelengths (e.g. Andre et al. 1990; Looney et al. 2000; Ward-Thompson et al. 2011; Murillo et al. 2013, 2018a,b; Harris et al. 2018; Hsieh et al. 2020; Ohashi et al. 2022; Codella et al. 2022; Mercimek et al. 2023, and references therein), revealing four protostars: VLA1623 A, which in turn is a Class 0 binary protostar (A1 and A2) with a separation of ~ 30 au, and surrounded by a circumbinary disk (CBD); VLA1623 B, a Class 0 protostar at ~ 130 au from VLA1623 A; VLA1623 W, a Class I protostar located at ~ 1300 au west of the VLA1623 A1+A2+B system.

Complex gas kinematics characterize VLA1623. The VLA1623 A binary system drives blue- and red-shifted outflows revealed in CO and H_2 emission (e.g., Andre et al. 1990; Hsieh et al. 2020; Hara et al. 2021) along the NW-SE direction. A rotating cavity opened by the mass loss process has been imaged in CS, CCH, and H^{13}CO^+ by Ohashi et al. (2022). Santangelo et al. (2015) detected a fast jet driven by VLA1623 B. Murillo et al. (2018b) and Ohashi et al. (2022) mapped a cold rotating cloud enveloping VLA1623 A and B in several simple species (e.g. DCO^+ and H^{13}CO^+). Recent ALMA studies imaged also molecular streamers infalling towards the A+B system in SO and C^{18}O lines (Hsieh et al. 2020; Mercimek et al. 2023). In the context of FAUST, Codella et al. (2022) mapped complex organic molecules, such as methanol (CH_3OH) and methyl formate (HCOOCH_3), which probe the circumstellar rotating gas around VLA1623 A1 and B. The detected rotation signatures suggest that the VLA1623 system is unstable: VLA1623 B counter-rotates with respect to the disk/envelope of VLA1623 A (e.g., Ohashi et al. 2022; Codella et al. 2022). Moreover, Murillo et al. (2013) and Mercimek et al. (2023) discuss the possibility that the protostellar source VLA1623 W, which is located ~ 1300 au West to the A1+A2+B system and shows a systemic velocity which differs by 2.2 km s^{-1} , has been ejected from the close triple system.

3 OBSERVATIONS

The VLA1623 protostellar system was observed between December 2018 and March 2020 by ALMA using Band 6 observations (216–234 GHz) in the context of the FAUST Large program (2018.1.01205.L; PI: Satoshi Yamamoto). Observations were conducted using two setups in Band 6 and one in Band 3. We used the 7-m array of the Atacama Compact Array (ACA) and the 12-m C43-4 and C43-1 configurations centering the observations at $\alpha_{2000} = 16^{\text{h}}26^{\text{m}}26^{\text{s}}.392$, $\delta_{2000} = -24^{\circ}24'30''.69$. In this paper, we analyse only the observations in Band 6, i.e. in Setup 1 (214.0–219.0 GHz and 229.0–234.0 GHz) and Setup 2 (242.5–247.5 GHz and 257.2–262.5 GHz). Table 1 reports the spectral parameters (transition, frequency, ν , upper-level energy E_{up} , and line strengths, $S\mu^2$) of the lines analysed in this paper: p- H_2CO ($3_{0,3} - 2_{0,2}$) (hereafter H_2CO), HDCO ($4_{1,4} - 3_{1,3}$), HDCO ($4_{2,2} - 3_{2,1}$), o- D_2CO ($4_{0,4} - 3_{0,3}$), and o- D_2CO ($4_{2,3} - 3_{2,2}$) (hereafter D_2CO). The molecular lines were observed with a bandwidth of 59 MHz ($76\text{--}80 \text{ km s}^{-1}$) and a resolution of 122 kHz ($\sim 0.17 \text{ km s}^{-1}$), with the exception of the HDCO ($4_{1,4} - 3_{1,3}$) and o- D_2CO ($4_{2,3} - 3_{2,2}$) lines which were

Species	Transition ^a	ν ^a (MHz)	E_{up} ^a (K)	$S\mu^2$ ^a (D ²)	rms (mJy beam ⁻¹)	δV (km s ⁻¹)	Beam size ('' × '')	Beam PA (°)	FoV ^b ('')
p-H ₂ CO	3 _{0,3} – 2 _{0,2}	218222.2	21	16	4.4	0.2	0.55 × 0.45	–74	24
HDCO	4 _{1,4} – 3 _{1,3}	246924.6	38	20	0.7	1.2	0.50 × 0.47	–77	21
HDCO	4 _{2,2} – 3 _{2,1}	259034.9	63	16	2.0	0.2	0.50 × 0.47	–95	20
o-D ₂ CO	4 _{0,4} – 3 _{0,3}	231410.2	28	43	2.3	0.2	0.50 × 0.43	–72	23
o-D ₂ CO	4 _{2,3} – 3 _{2,2}	233650.4	50	33	1.0	0.6	0.51 × 0.42	–75	23

Table 1. List of the observed lines towards VLA1623–2417. ^a Spectroscopic parameters are taken from the CDMS catalog (Müller et al. 2005). ^b The FWHM of Field of View. However the ALMA images cover larger area than FoV.

observed at lower spectral resolution in the broad spectral windows for the continuum (bandwidth of 1.9 GHz, and resolution of 1.2 and 0.6 km s⁻¹, respectively).

For each configuration, line-free continuum emission was used for self-calibration. We subtracted the continuum model derived from the self-calibration to produce continuum-subtracted line data. The quasars J1427-4206, J1517-2422, J1625-2527, J1924-2914, and J1626-2951 were used to calibrate the data, with a final absolute flux calibration uncertainty of ~10%. We used a modified version of the calibration pipeline¹ within CASA 5.6.1-8 (CASA Team et al. 2022), including an additional calibration routine to correct for T_{sys} issues and spectral data normalization².

After merging the 12m and 7m configurations, continuum subtracted line cubes were cleaned using the task *tclean*. We adopted Briggs robustness parameter of 0.5 for molecular lines, while the parameter is -2.0 for the bright continuum to obtain the highest angular resolution. Primary beam corrections were also applied. The size and position angle (PA) of the synthesized beam, and the root mean square noise (r.m.s.) of the continuum maps in Setup 1 and Setup 2 are respectively: 0''.42 × 0''.32, PA=–65°, 0.26 mJy beam⁻¹ and 0''.38 × 0''.34, PA=67°, 0.27 mJy beam⁻¹. The details of the continuum-subtracted line datacubes are listed in Table 1: the r.m.s., the spectral resolution (δV), the synthesized beam size and PA, and the field of view (FoV).

4 RESULTS

We detected emission from all the transitions of H₂CO and its isotopologues listed in Table 1. Figure A1 shows the spectra of the detected transitions (in brightness temperature scale, T_{B}) obtained by integrating the emission over the FoV.

Figure 1 shows moment 0 maps, i.e., the spatial distribution of the lines emission integrated over the emitting velocity range. The continuum emission at 1.3 mm is shown by magenta contours to pinpoint the positions of the A1 and A2 sources (not disentangled at the FAUST spatial resolution), their circumbinary disk, and the B and W protostars (see also the FAUST continuum maps reported by Codella et al. 2022, 2024; Mercimek et al. 2023). In the following subsections, we analyse the H₂CO, HDCO, and D₂CO emission and identify the structures probed by these species.

¹ https://github.com/autocorr/faust_line_imaging; Chandler et al. (in preparation)

² <https://help.almascience.org/kb/articles/what-errors-could-originate-from-the-correlator-spectral-normalization-and-tsys-calibration>; Moellenbrock et al. (in preparation)

4.1 H₂CO emission

Figure 1 (Upper-Left) shows the moment 0 map of H₂CO (3_{0,3} – 2_{0,2}) emission. We detect compact H₂CO emission towards all the protostars in the field, i.e. VLA1623 A, B, and W. In addition, formaldehyde probes extended structures: the envelope of the VLA1623 A+B system, the cavities opened by the outflow driven by VLA1623 A and first imaged in CS 5 – 4 by Ohashi et al. (2022), and a bright elongated structure south of VLA1623 W. In the following, we discuss the properties of both compact and extended emissions by focusing on the channel maps of H₂CO emission on both small scales (Sect. 4.1.1), and large scales (4.1.2).

4.1.1 Compact H₂CO emission towards VLA1623 A, B, and W

The inspection of the channel maps of H₂CO allows us to reveal structures emitting only in selected velocity ranges, otherwise diluted in the moment 0 map. Figure 2 shows a zoom-in of the H₂CO (3_{0,3} – 2_{0,2}) emission on the ~ 300 au region around the VLA1623 A and B sources. The emission towards the A and B protostars is compact and spatially unresolved (≤ 50 au) at high-velocity, i.e. at blue- and red-shifted velocities larger than 2 km s⁻¹ with respect to the systemic velocity of the A and B sources, ($V_{\text{sys}} = +3.8$ km s⁻¹, Ohashi et al. 2022) and shows velocity gradients, suggestive of rotation. In particular, VLA1623 A shows red-shifted compact emission SW to the continuum peak (at [+5.8, +6.8] km s⁻¹, i.e. up to +3 km s⁻¹ with respect to V_{sys}), and blue-shifted emission on the opposite side ([+0.4, +1.8] km s⁻¹, i.e. up to –4.2 km s⁻¹ with respect to V_{sys}). The velocity gradient towards VLA1623 B is roughly along the same direction but is inverted (redshifted on the NE, and blue-shifted on the SW), and reach higher radial velocities, up to +10.0 km s⁻¹, and –5.2 km s⁻¹ (i.e. up to +6.2 km s⁻¹ and –9 km s⁻¹ with respect to V_{sys}). Remarkably, the velocity gradients observed towards VLA1623 A and VLA1623 B are along the PA of their disks (~ 48 – 49° for VLA1623 A1 and A2, and ~ 42° for VLA1623 B, from the high-resolution continuum maps by Harris et al. 2018), and are consistent with those shown in CS 5 – 4 (Ohashi et al. 2022). Codella et al. (2022) observed the same velocity gradients in CH₃OH lines towards A and B, suggesting that methanol probes the hot corinos (where dust mantles are sublimated at temperatures ≥ 100 K) or the outer regions of the protostellar disks, where infalling gas from the envelope causes low-velocity shocks sputtering the dust (Sakai et al. 2014a,b). However, the maximum radial velocities of H₂CO emission are smaller than those observed using CH₃OH (up to +7 km s⁻¹ and –2 km s⁻¹ for VLA1623 A, and +14 km s⁻¹ and –10 km s⁻¹ for VLA1623 B), suggesting that formaldehyde emission originates from a more extended portion of the envelopes/disks associated with the A and B sources, with respect to methanol. To conclude, the high-velocity H₂CO emission traces the counter-rotating envelopes around the A1+A2 binary system, and VLA1623 B. Note that Fig.

VLA1623–2417

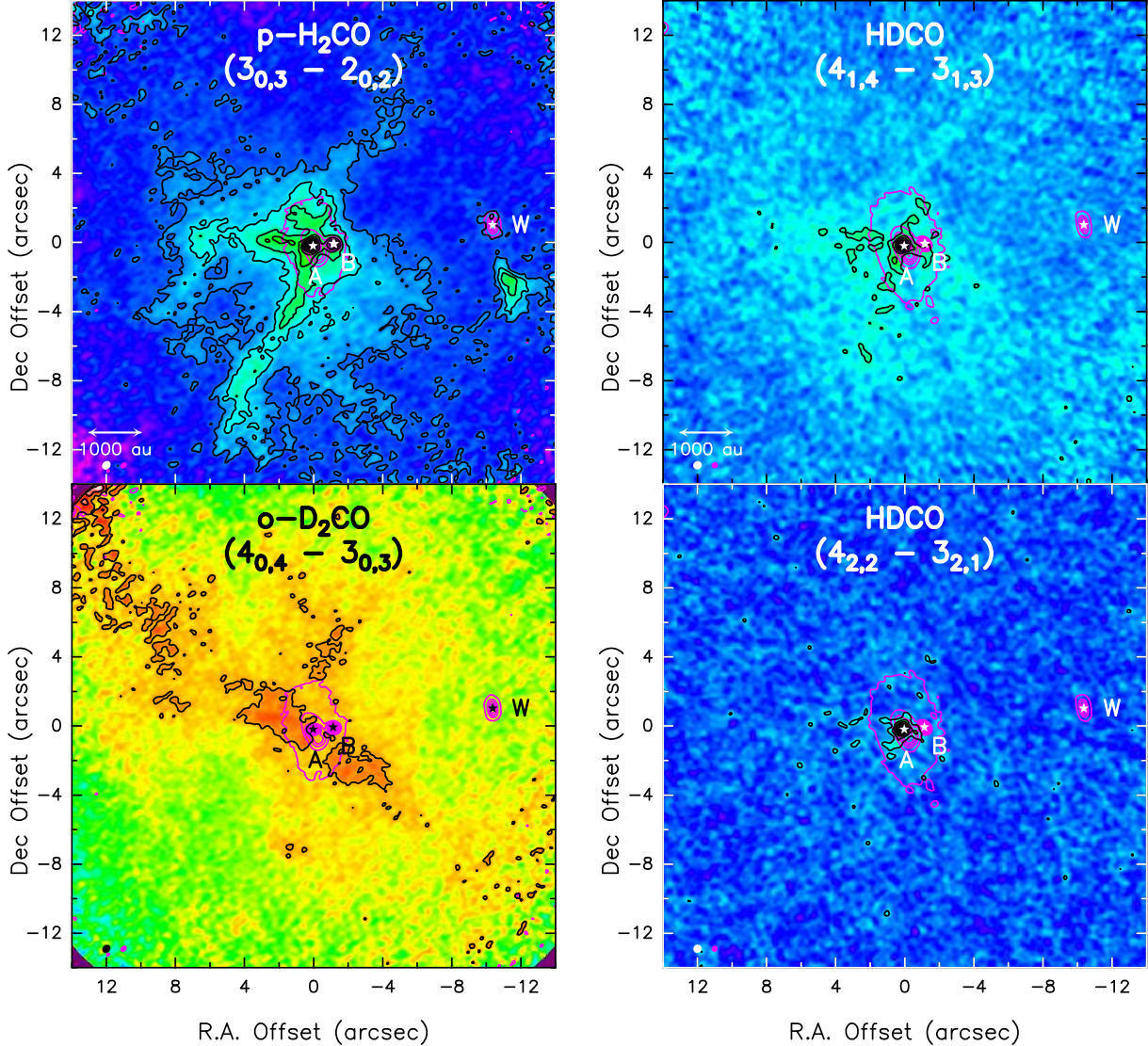


Figure 1. Integrated intensity (moment 0) maps of H_2CO ($3_{0,3} - 2_{0,2}$), HDCO ($4_{1,4} - 3_{1,3}$), HDCO ($4_{2,2} - 3_{2,1}$), and D_2CO ($4_{0,4} - 3_{0,3}$) towards VLA 1623–2417. The maps have been obtained by integrating in the velocity range of $[-5.2, +10.0]$, $[+0.0, +6.2]$, $[+0.0, +6.2]$, and $[+3.0, +5.0]$ km s^{-1} , respectively. The white and black stars indicate the A, B, and W protostars. The first black contours and steps correspond to 3σ : 24.0, 15.0, 9.0, and 15.0 $\text{mJy km s}^{-1} \text{beam}^{-1}$ for H_2CO ($3_{0,3} - 2_{0,2}$), HDCO ($4_{1,4} - 3_{1,3}$), HDCO ($4_{2,2} - 3_{2,1}$), and D_2CO ($4_{0,4} - 3_{0,3}$), respectively. The magenta contours are for the dust continuum emission at 1.3 mm. For the continuum in Setup 1, which is shown in the H_2CO and D_2CO maps, the first contour and steps are 3σ ($0.78 \text{ mJy beam}^{-1}$) and 20σ , respectively. For the continuum in Setup 2, shown in the two HDCO maps, the first contour is 3σ ($0.81 \text{ mJy beam}^{-1}$) with steps of 20σ . The ellipses in the left bottom corners show the synthesized beams: in white and black for line emission (see Table 1) and in magenta for continuum emission.

2 shows absorption towards the continuum peak of VLA1623 A and B, at velocities close to V_{sys} , plausibly due to line absorption along the line of sight and optically thick dust (see Sect. 5.1).

Finally, Fig. 3 shows the H_2CO ($3_{0,3} - 2_{0,2}$) channel maps in the ~ 300 au region centered at the position of the VLA1623 W protostar. The maps show spatially unresolved (≤ 50 au) blue-shifted emission north of source W, up to velocities of -3 km s^{-1} with respect to the systemic velocity of VLA1623 W ($V_{\text{sys}}(\text{W}) = +1.6 \text{ km s}^{-1}$, Mercimek et al. 2023). This emission is consistent with the blue side of the inner envelope rotating along the N-S direction revealed by Mercimek et al. (2023) using the C^{18}O 2-1 line. The non-detection of the southern red-shifted side in H_2CO is consistent

with the C^{18}O emission, which is brighter in the blue-shifted lobe than in the red-shifted one.

The compact H_2CO emissions towards the three protostars VLA1623 A, B, and W (labeled as A, B, and W), and the velocity ranges of emission are summarized in Table 2.

4.1.2 Streamers and Outflow Cavities in H_2CO emission

Figure 4 shows the H_2CO ($3_{0,3} - 2_{0,2}$) velocity channel maps over a larger region ($\sim 24'' \times 24''$) with respect to what reported in Sect. 4.1.1. As references, we draw in magenta the outflow cavity walls probed by CS(5–4) emission (Ohashi et al. 2022), and the dust continuum emission at 1.3 mm. Several extended structures are

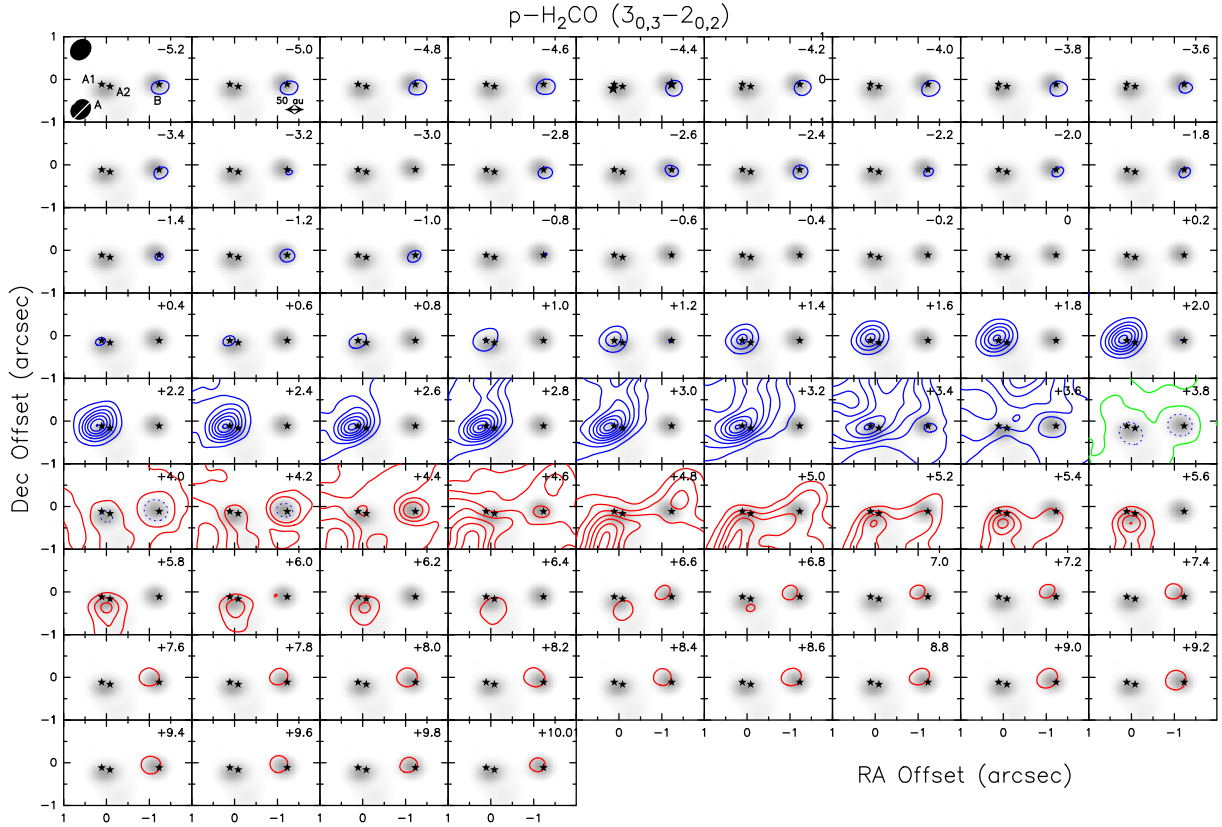


Figure 2. Channel maps of the H_2CO ($3_{0,3} - 2_{0,2}$) emission in the ~ 300 au region around the VLA1623 A1+A2 and B protostars (marked by the black stars). The LSR velocity is labeled in the top-right corner of each channel. The contours of the emission are green in the channel at systemic velocity and blue/red in the channels at blue-/red-shifted velocities with respect to the systemic velocity of VLA1623 A and B ($+3.8 \text{ km s}^{-1}$; Ohashi et al. 2022). The first contours and steps are 3σ ($13.2 \text{ mJy km s}^{-1} \text{ beam}^{-1}$). The grayscale background shows the 1.3 mm continuum emission in Setup 1. The dashed blue contour in the channels between $+3.8$ and $+4.2 \text{ km s}^{-1}$ shows negative line intensity (absorption). The synthesized beams are shown in the top-left channel by filled and dashed ellipses for line and continuum emission, respectively.

detected in H_2CO . Table 2 lists these structures, and the velocity ranges over which they are detected in the channel maps, moving from blue-shifted to red-shifted velocities, and labeling them from I to VII:

- **(I)** in the $[+0.8, +2.2] \text{ km s}^{-1}$ velocity channels, we detect H_2CO emission at the northern edge of the circumbinary disk surrounding VLA1623 A1+A2. This component has already been detected in SO lines by Hsieh et al. (2020) and Codella et al. (2024). They suggested that this feature is associated with an accretion shock produced by a blue-shifted streamer infalling onto the circumbinary disk (component V, see below);

- **(II)** the emission on the $[+1.4 \text{ and } +2.2] \text{ km s}^{-1}$ velocity range reveals an extended structure located south to VLA1623 A. This component, already imaged in SO lines by Codella et al. (2024), is a blue-shifted streamer infalling on the VLA1623 B protostar. Although the position of the streamer (projected on the plane of the sky) could suggest its association with the southern outflow cavity of VLA1623 A, this is excluded by the fact that the accretion streamer is blue-shifted while the southern cavity side is red-shifted;

- **(III)** a streamer connecting the southern region around A+B with the VLA1623 W protostar is detected in the $[+1.8, +3.2] \text{ km s}^{-1}$ velocity range. The streamer is red-shifted with respect to the systemic velocity of the W object ($+1.6 \text{ km s}^{-1}$; Mercimek et al. 2023). This streamer has been previously detected in C^{18}O by Mer-

cimek et al. (2023). The H_2CO emission traces the streamer without the contamination of the A+B envelope emitting in C^{18}O ;

- **(IV)** the $[+2.4, +3.2] \text{ km s}^{-1}$ velocity range shows an additional elongated structure SW of VLA1623 W. This structure is detected close to the half-power point of the primary beam, therefore no reliable conclusion on its origin can be drawn;

- **(V)** a slightly blue-shifted streamer extending from the North edge of the FoV to NW and then pointing towards VLA1623 A is imaged in the $[+2.8, +3.6] \text{ km s}^{-1}$ velocity range. This emission likely traces a streamer infalling onto the circumbinary system and causing an accretion shock, whose emission is labeled as I. This scenario has already been suggested by Hsieh et al. (2020) based on SO and C^{18}O lines.

- **(VI)** at velocities close to the systemic velocity of VLA1623 A and B, i.e. in the $[+3.4, +4.4] \text{ km s}^{-1}$ velocity range, H_2CO emission probes the region encompassed by the rotating outflow cavities first imaged in CS 5 – 4 by Ohashi et al. (2022). The association with the outflow cavity is confirmed by kinematics: the northern side is blue-shifted, while the southern side is red-shifted, in agreement with CS emission. The H_2CO emission as a probe of outflow cavities has been reported also by Sabatini et al. (2024) for the outflow associated with the IRS7B protostellar system in the Corona Australis.

- **(VII)** a red-shifted elongated structure south of VLA1623 A is detected at $[+4.4, +5.0] \text{ km s}^{-1}$ velocities, which is not coincident with the southern outflow cavities. This emission component is per-

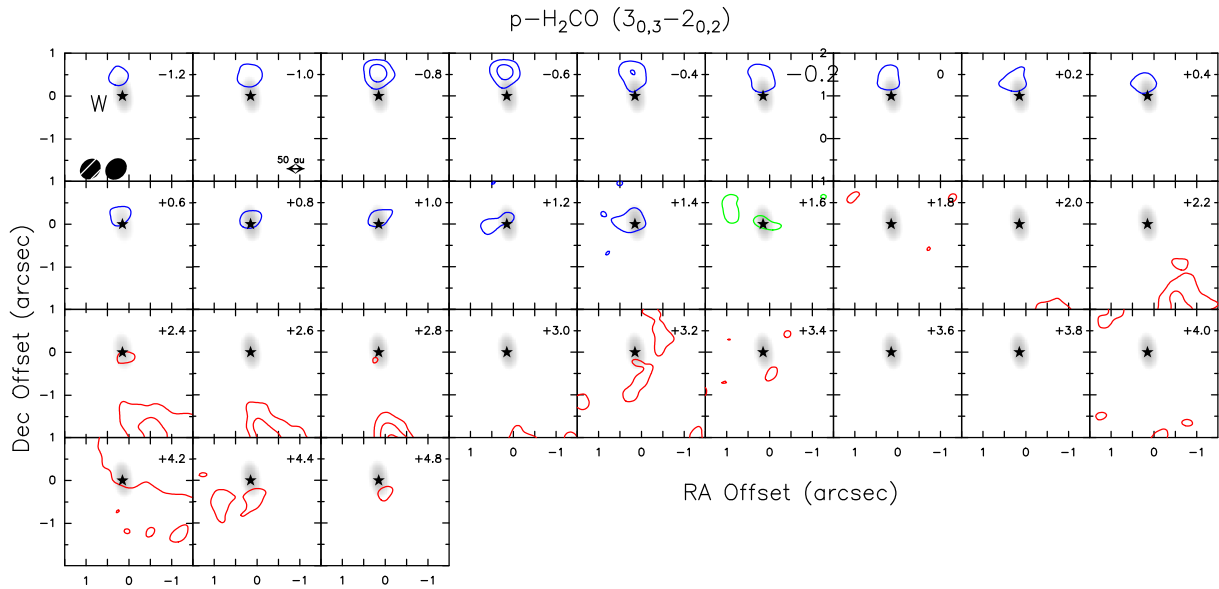


Figure 3. Channel maps of the H_2CO ($3_{0,3} - 2_{0,2}$) emission in the ~ 300 au region around the VLA1623 W protostar (marked by the black star). The LSR velocity is labeled in the top-right corner of each channel. The contours of the emission are green in the channel at systemic velocity and blue/red in the channels at blue-/red-shifted velocities with respect to the systemic velocity of VLA1623 W ($+1.6 \text{ km s}^{-1}$ Mercimek et al. 2023). The first contours and steps are 3σ ($13.2 \text{ mJy km s}^{-1} \text{ beam}^{-1}$). The grayscale background shows the 1.3 mm continuum emission in Setup 1. The synthesized beams are shown in the top-left channel by filled and dashed circles for line and continuum emission, respectively.

pendicular to the outflow direction, and is plausibly associated with a streamer infalling onto the VLA1623 A and B protostars. Hsieh et al. (2020) has previously reported this structure, proposing the occurrence of an accretion streamer feeding the (red-shifted) southern side of the circumbinary disk around VLA1623 A.

4.2 HDCO emission

The moment 0 maps of the HDCO ($4_{1,4} - 3_{1,3}$) and ($4_{2,2} - 3_{2,1}$) lines are shown in Fig. 1, while the channel maps over a small ($\sim 3'' \times 2''$) and large ($\sim 19'' \times 16''$) region are shown in Fig. A2 and A3. The maps show no HDCO emission detected toward VLA1623 B and W, while the emission towards VLA1623 A consists of several components.

In Figure 5 we show the HDCO emission integrated over selected velocity intervals, i.e. at systemic velocity ($V_{\text{sys}} = +3.8 \text{ km s}^{-1}$, left panels); at low-velocity (up to $\pm 1.2 \text{ km s}^{-1}$ with respect to V_{sys} , middle panels); and at high velocity (up to $\pm 3.0 \text{ km s}^{-1}$ with respect to V_{sys} , right panels). The figure shows that some of the components identified in the analysis of the H_2CO channel maps are also associated with HDCO emission, namely:

- **(A)** the high-velocity HDCO emission is compact around the A1+A2 binary system, and show a velocity gradient along the NE-SW direction, in agreement with H_2CO (see Fig. 2), and CH_3OH (Codella et al. 2022). As for H_2CO , the HDCO compact emission is at lower velocities than methanol, thus it probes a more extended region of the rotating envelope around VLA1623 A (see Sect. 4.1.1);
- **(VI)** the HDCO emission at systemic velocity and low blue- and red-shifted velocities traces the rotating outflow cavities driven by VLA1623 A, in agreement with CS and H_2CO emission (Ohashi et al. 2022);
- **(V, VII)** the lower excitation HDCO ($4_{1,4} - 3_{1,3}$) line ($E_{\text{u}} = 38 \text{ K}$), which is brighter, also shows low-velocity emission north and south of VLA1623 A, which is not associated with the outflow

cavities. Despite the low S/N ($\sim 3\sigma$) of the HDCO channel maps, we identify that the low-velocity emission is associated with the northern blue-shifted and southern red-shifted streamers infalling on VLA1623 A and revealed by H_2CO (components V and VII, see Table 2).

4.3 D_2CO emission

The moment 0 map of the D_2CO lower excitation line ($4_{0,4} - 3_{0,3}$) is shown in Fig. 1, while Figure 6 shows the velocity channel maps, with overplot the outflow cavities revealed by CS emission (Ohashi et al. 2022), and the dust continuum emission at 1.3 mm. Table 2 lists the detected structures, moving along the velocity channel maps from blue-shifted to red-shifted velocities, and labeling them from V to VII. As for HDCO, D_2CO shows no emission towards the VLA1623 B and W protostars (components B and W in Table 2), while faint emission from the inner envelope of VLA1623 A is recovered in the spectrum extracted at the source continuum peak (see Sect. 5.1). Surprisingly, the D_2CO moment 0 map and channel maps reveal a spatial distribution which is different than that of HDCO and H_2CO : the D_2CO emission close to systemic velocity ($V_{\text{sys}} \pm 1 \text{ km s}^{-1}$) extends out to the edges of the field of view, and probe a region which does not coincide with the wide-angle outflow cavities outlined by the CS emission. Figure A4 compares the spatial distributions of H_2CO and D_2CO in selected velocity ranges, and allows us to identify some of the structures detected in H_2CO and reported in Table 2. More specifically, D_2CO probes the following components:

- **(V)** on the $[+3.2, +3.6] \text{ km s}^{-1}$ velocity range (Panel a) the D_2CO emission is partially coincident with the northern blue-shifted streamer revealed by H_2CO . However, the peak of the D_2CO emission is at the edges of the H_2CO structure;
- **(VI)** the D_2CO emission on the $[+3.4, +4.4] \text{ km s}^{-1}$ velocity range (Panel b) traces the outflow cavities detected in H_2CO . Note

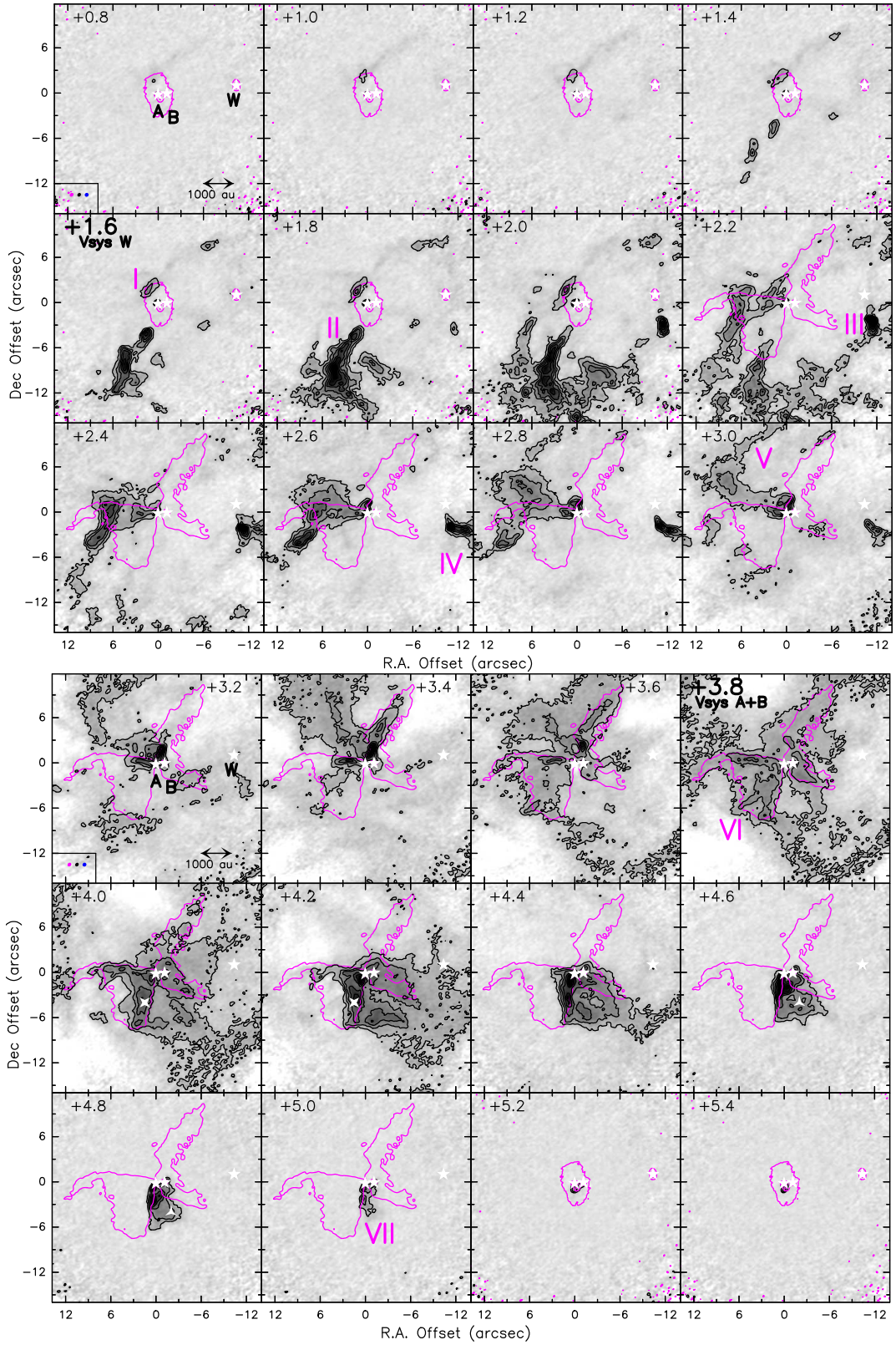


Figure 4. Channel maps of the H_2CO ($3_{0,3} - 2_{0,2}$) emission in the velocity range $[+0.8, +5.4] \text{ km s}^{-1}$. The first contour is at 3σ , and the step is 3σ . The magenta contours in the channels from $+2.2 \text{ km s}^{-1}$ to $+5.0 \text{ km s}^{-1}$ indicate the outflow cavity walls probed by CS ($5-4$) emission (25σ contour, from [Ohashi et al. 2022](#)). The magenta contour in the channels from $+0.8 \text{ km s}^{-1}$ to $+2.0 \text{ km s}^{-1}$ and from $+5.2 \text{ km s}^{-1}$ to $+5.4 \text{ km s}^{-1}$ indicate the dust continuum emission at 1.3 mm , starting from 3σ ($0.78 \text{ mJy beam}^{-1}$) with intervals of 40σ . The synthesized beams are shown by the magenta, black, and blue ellipses in the bottom-left corner of the first channel for H_2CO , continuum, and CS ($5-4$) emission, respectively. The positions of VLA1623 A, B, and W are indicated by the white stars and are labeled in the first channel. The large-scale emission components listed as "I", "II", "III", "IV", "V", "VI", and "VII" in Table 2 are labeled. Cross and triangle symbols in the channels at $+4.0 \text{ km s}^{-1}$, $+4.2 \text{ km s}^{-1}$, and $+4.6 \text{ km s}^{-1}$ indicate the positions along the outflow cavity wall and the streamer where the line spectra are extracted (see Fig. 8 in Sect. 5.1).

Label	Component	H ₂ CO (km s ⁻¹)	HDCO (km s ⁻¹)	D ₂ CO (km s ⁻¹)	Spectrum Position (<i>l</i> , <i>b</i>)
COMPACT					
A	inner rotating envelope of A	[+0.4, +1.8] [+5.8, +6.8]	[+0.8, +2.6] [+5.0, +6.8]	–	(0, 0)
B	inner rotating envelope of B	[–5.2, –1.0] [+6.6, +10.0]	–	–	(–1.16, +0.11)
W	inner rotating envelope of W	[–1.2, +1.6] –	– –	– –	(–10.32, +1.26)
EXTENDED					
I	accretion shock at the northern edge of A CBD	[+0.8, +2.2]	–	–	–
II	southern blue-shifted streamer towards B	[+1.4, +2.2]	–	–	–
III	southern red-shifted streamer towards W	[+1.8, +3.2]	–	–	–
IV	SE elongated emission associated with W	[+2.4, +3.2]	–	–	–
V	northern blue-shifted streamer towards A	[+2.8, +3.6]	[+2.6, +3.8]	[+3.2, +3.6]	–
VI	outflow cavities driven by A	[+3.4, +4.4]	[+2.6, +5.0]	[+3.4, +4.4]	(+1.49, –3.78)
VII	southern red-shifted streamer towards A	[+4.4, +5.0]	[+3.8, +5.0]	[+4.4, +5.0]	(–2.01, –3.78)

Table 2. Compact and extended emission components towards VLA1623-2417 identified in H₂CO, HDCO, and D₂CO channel maps in the listed velocity ranges. The positions (R.A. and Dec. offsets with respect to VLA1623 A) where the spectra of the identified components are extracted are listed in the last column.

that the D₂CO emission at low velocities looks more contaminated by extended emission plausibly associated with the large-scale envelope;

- **(VII)** the D₂CO emission on [+4.4, +5.0] km s⁻¹ velocity range (Panel c) appears associated with the southern red-shifted streamer labeled as VII in the H₂CO channel maps. Figure A7 shows the intensity-weighted mean velocity (moment 1) map of D₂CO (4_{0,4} – 3_{0,3}) emission, where the red-shifted streamer infalling on the VLA1623 A system from the SE is clearly outlined. However, also in this case, the emission peaks of H₂CO and D₂CO are not collocated, with H₂CO mainly associated with the eastern side of the VII structure and D₂CO mainly emitted from the western side.

The higher excitation D₂CO (4_{2,3} – 3_{2,2}) line ($E_{\text{up}} \sim 50$ K) is also marginally detected. The channel maps (Fig. A5) show emission at very low S/N ($\sim 2-3\sigma$), but tentatively suggest a spatial distribution consistent with that of the brighter lower-excitation D₂CO line (4_{0,4} – 3_{0,3}). The maps show signatures of the outflow cavities at systemic velocity (+3.8 km s⁻¹), and of the southern red-shifted streamer at +4.4 km s⁻¹ (labeled as VI and VII in Table 2). Despite the low S/N, the D₂CO (4_{2,3} – 3_{2,2}) line is clearly detected in the spectrum obtained by integrating the emission over a 10'' region centered on VLA1623 A (see Fig. 7). The line profile is in agreement with the profile of the lower excitation (4_{0,4} – 3_{0,3}) line (see Fig. 8), peaking in the same velocity range (3.8 – 4.4 km s⁻¹).

5 DISCUSSION

The analysis of the channel maps presented in Sect. 4 showed that H₂CO and its deuterated isotopologues trace several components of the VLA1623 protostellar system: the inner protostellar envelopes, the outflow cavities, and the accretion streamers. VLA1623 is therefore an excellent laboratory to study the D/H ratio in these different components. The derivation of the D/H values is reported in Sect. 5.1, while in Sect. 5.2 we compare the estimated D/H ratios with values derived for other sources in the literature.

In addition, within a fixed emitting velocity range, H₂CO, HDCO, and D₂CO do not always show the same spatial distribution. The origin of this difference will be discussed in Sect. 5.3.

5.1 Deuteration in the inner envelope, in the outflow cavities, and in the streamers

Figure 8 shows the spectra (in T_{B} scale) of the observed H₂CO, HDCO, and D₂CO lines (see Tab. 1), extracted in five selected positions representative of the compact and extended components identified towards the VLA1623-2417 cluster: at the dust continuum peaks of the protostellar sources VLA1623 A, B, and W (components A, B, and W in Table 2); at a representative position of the SE outflow cavity (VI component); and at a representative position of the red-shifted southern streamer (VII component). The R.A. and Dec. offset of the selected positions are listed in Tab. 2, and marked in Figs. 4, 5, 6.

Different positions are associated with different line profiles, reflecting the kinematical components shown by the channel maps analysed in Sect. 4:

- The spectra extracted at the position of the VLA1623 A continuum peak exhibit a narrow absorption feature at systemic velocity detected in the lower excitation H₂CO and D₂CO lines ($E_{\text{up}} = 21$ K, and 28 K). This is due to absorption by the cold gas along the line of sight and by the optically thick dust continuum emission. The spectra shows blue-shifted and red-shifted emission, which probe the inner rotating envelope of A. In addition, the lines profiles are asymmetric with the blue-shifted emission more intense than the red-shifted one, suggestive of infall.

- The H₂CO spectrum toward VLA1623 B shows symmetric red-shifted and blue-shifted emission out to $\sim \pm 10$ km s⁻¹ with respect to the systemic velocity (+3.8 km s⁻¹), which probes the inner portion of the rotating envelope of B, consistently with the H₂CO channel maps (Fig. 2). As for the spectra towards VLA1623 A, the lower excitation H₂CO and D₂CO lines exhibit a narrow absorption feature at systemic velocity due to absorption by the cold gas along the line of sight and by the optically thick dust continuum emission. This absorption feature has been also observed in the CS, CCH, and H¹³CO⁺ low excitation lines ($E_{\text{up}} = 25-35$ K) toward VLA1623 B (Ohashi et al. 2022). In addition, the H₂CO spectrum shows a red-shifted excess, also observed in HDCO, which originates from the NW red-shifted side of the rotating outflow cavity associated with VLA1623 A (labeled as NW Outflow Cavity in Table 3).

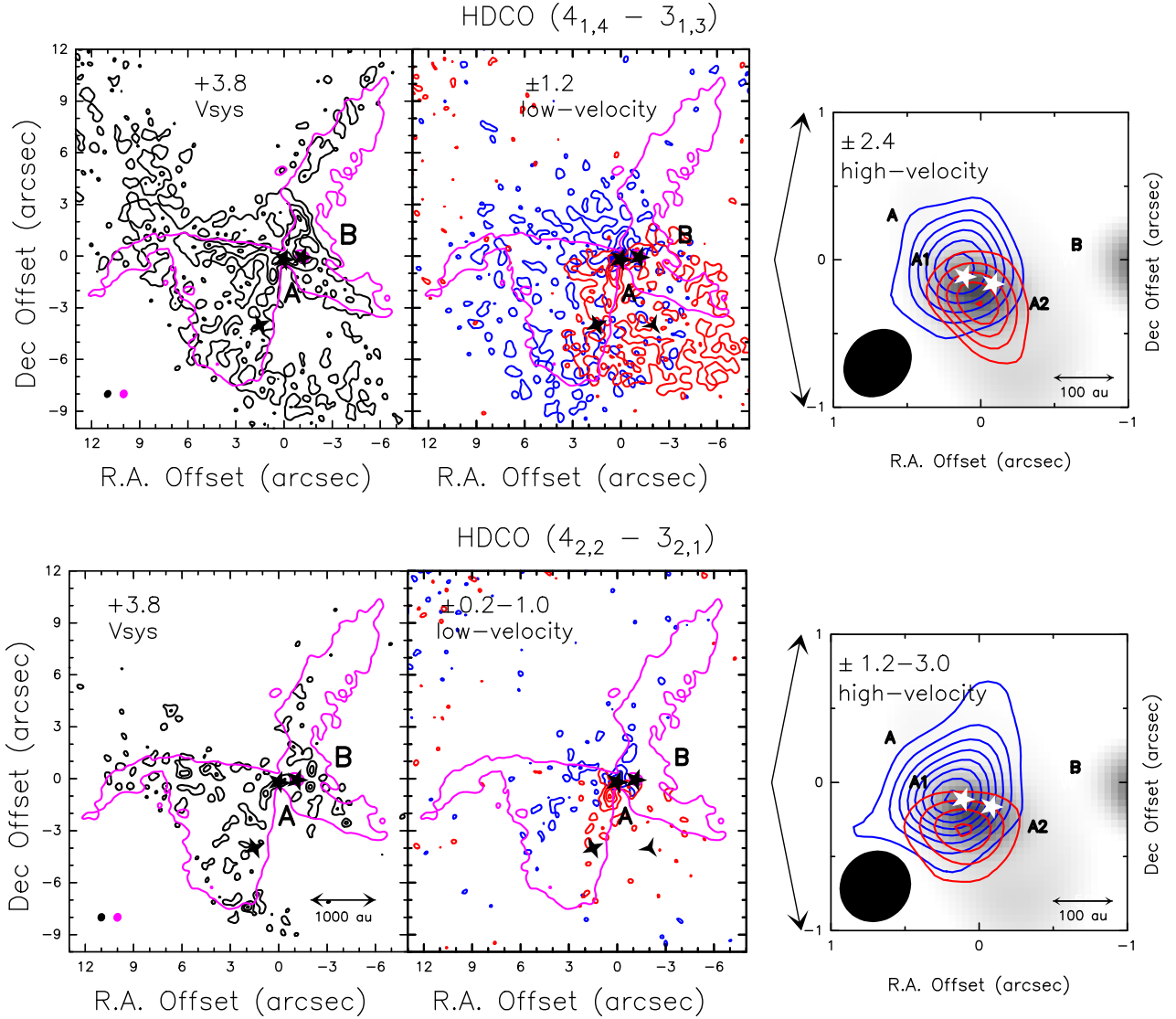


Figure 5. Velocity-integrated maps of HDCO lines towards VLA1623. *Top row:* HDCO ($4_{1,4} - 3_{1,3}$). The left panel shows the emission at systemic velocity ($+3.8 \text{ km s}^{-1}$, in black contours), the middle and right panels show low-velocity ($\pm 1.2 \text{ km s}^{-1}$) and high-velocity ($\pm 2.4 \text{ km s}^{-1}$) emission (red and blue contours). The first contours and steps are 3σ ($2.1 \text{ mJy beam}^{-1}$). *Bottom row:* HDCO ($4_{2,2} - 3_{2,1}$). The left panel shows the emission at systemic velocity ($+3.8 \text{ km s}^{-1}$, in black contours), the middle and right panels show low-velocity ($[\pm 0.2, \pm 1.0] \text{ km s}^{-1}$) and high-velocity ($[\pm 1.2, \pm 3.0] \text{ km s}^{-1}$) emission (red and blue contours). The first contours and steps are 3σ (3σ is 6.0 and $6.0 \text{ mJy beam}^{-1}$ for low- and high-velocity maps, respectively). The white stars in the right panels (high-velocity emission maps) indicate the position of VLA1623 A1, A2 from Harris et al. (2018); the black stars in the other panels show the position of VLA1623 A and B from the FAUST continuum maps at 1.3 mm (Mercimek et al. 2023). The magenta contours show the CS ($5-4$) emission which probes the outflow cavity walls (25σ contour, from Ohashi et al. 2022). The grayscale background shows the 1.3 mm continuum emission in Setup 2. The HDCO and CS synthesized beams are shown in black and magenta in the bottom-left of the left and right panels. Cross and triangle symbols in the left and middle panels show the positions of the outflow cavity and streamer where the spectra are extracted (see Fig. 8 in Sect. 5.1).

- The H_2CO spectrum towards VLA1623 W shows blue-shifted emission, unveiling the blue-shifted northern side of the inner rotating envelope of W, as illustrated in Fig. 2, which is brighter than the red-shifted one consistent with the observations of C^{18}O by Mercimek et al. (2023). No emission is detected in HDCO and D_2CO .

- The H_2CO spectrum extracted at the position along the SE outflow cavity (component VI) peak at systemic velocity and shows a counterpart in the HDCO and D_2CO spectra. In addition, the spectrum shows a blue-shifted emission component, which probes the southern blue-shifted streamer (component II), which spatially overlaps with the cavity. This component is also detected in HDCO.

- The spectra extracted at the position of the southern red-shifted

streamer (component VII) exhibits a narrow ($0.6\text{--}0.8 \text{ km s}^{-1}$) nearly Gaussian emission component at red-shifted velocities in H_2CO , HDCO, and D_2CO .

Despite the narrow range of upper-level energies of the detected HDCO lines (38 K and 63 K), we used the intensity ratio of the two HDCO lines to determine the excitation temperature (T_{ex}) of the gas in the different components. Local thermodynamic equilibrium (LTE) and optically thin emission have been assumed. To properly measure the line intensities from the spectra extracted at the position of the continuum peaks of A and B and avoid the effect of absorption at systemic velocity, we integrated the emission on the blue-shifted

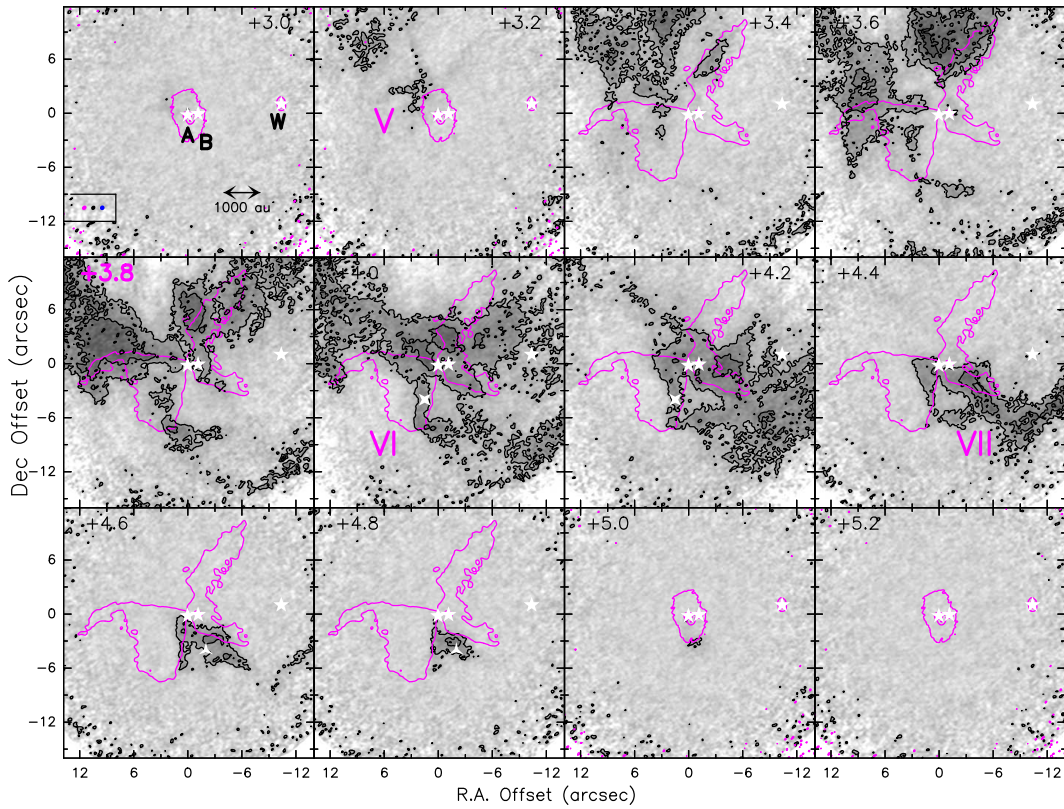


Figure 6. Channel maps of the D_2CO ($4_{0,4} - 3_{0,3}$) emission in the velocity range $[+3.0, +5.2]$ km s^{-1} . The first contour is at 3σ , and the step is 3σ . The magenta contours in the channels from $+3.4$ km s^{-1} to $+4.8$ km s^{-1} indicate the outflow cavity walls probed by CS ($5-4$) emission (25σ contour, from [Ohashi et al. 2022](#)). The magenta contour in the channels from $+3.0$ km s^{-1} to $+3.2$ km s^{-1} and from $+5.0$ km s^{-1} to $+5.2$ km s^{-1} indicate the dust continuum emission at 1.3 mm, starting from 3σ (0.78 mJy beam^{-1}) with intervals of 40σ . The synthesized beams are shown by the magenta, black, and blue ellipses in the bottom-left corner of the first channel for CS ($5-4$), continuum, and H_2CO , respectively. The positions of VLA 1623 A, B, and W are indicated by the white stars and are labeled in the first channel. The large-scale emission components are labeled as "V," "VI," and "VII" in Table 2, consistently with the H_2CO components. Cross and triangle symbols at channels between $+4.2$ and $+4.8$ km s^{-1} show where the spectra of outflow cavity wall and streamer are extracted (see Fig. 8 in Sect. 5.1).

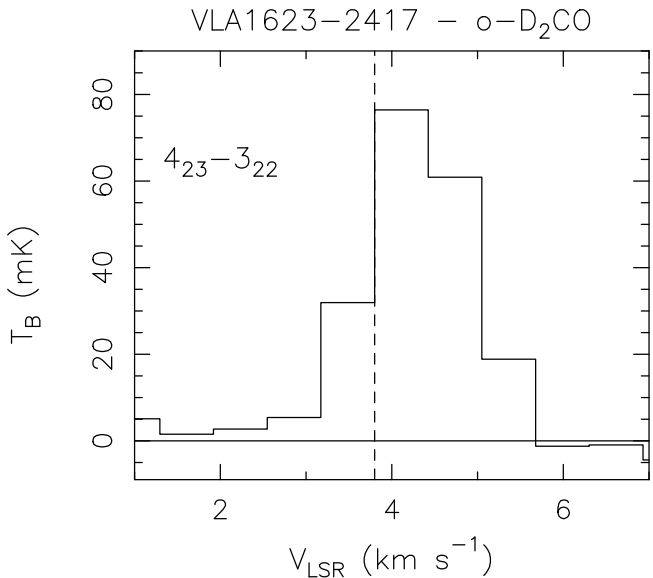


Figure 7. Spectral profile of D_2CO ($4_{2,3} - 3_{2,2}$) profile (in T_B scale), integrated on a $10''$ region centered on VLA1623 A. The dashed vertical line indicates the systemic velocity of VLA1623 A and B ($+3.8$ km s^{-1} , [Ohashi et al. 2022](#)).

and red-shifted velocity ranges highlighted in Fig. 8 by yellow bands. Table 3 reports, for each component, the velocity ranges used for integration, the obtained line integrated intensities, and the excitation temperature estimated from the HDCO line ratio.

The excitation temperature towards VLA1623 A is 125 ± 60 K, supporting the association of the observed line emission with the inner envelope heated by the VLA1623 A binary system. The excitation temperature in the SE outflow cavity is lower 37 ± 19 K. Low T_{ex} is obtained also towards VLA1623 B (28 ± 12 K), confirming that the HDCO emission detected towards B plausibly probes the redshifted side of the rotating outflow cavity as suggested by the maps in Fig. 5. Finally, the excitation temperature estimated in the streamers (II and VII) is an upper limit, due to the non-detection of the higher excitation HDCO line, and is ≤ 15 K. This is consistent with the expected temperatures at a separation of ~ 600 au from the protostars (see Tab. 2).

To determine the column densities of H_2CO , HDCO, and D_2CO , we assumed LTE and optically thin emission and adopted the excitation temperature (T_{ex}) estimated from the HDCO lines. This is based on the assumption that the three species probe the same component, an hypothesis reinforced by the similarity of the extracted line profiles at each position. As reported in Tab. 3, the HDCO column density towards VLA1623 A is $5 \pm 3 \times 10^{13}$ cm^{-2} , an order of magnitude higher than that measured in the VLA1623 B red-shifted and SE cavities, $N_{\text{HDCO}} \approx 5-6 \times 10^{12}$ cm^{-2} . The HDCO column densities

in the streamers II and VII are $\geq 10^{12} \text{ cm}^{-2}$. The formaldehyde column densities are $\approx 3 \times 10^{14} \text{ cm}^{-2}$ (VLA1623 A), and $3\text{--}8 \times 10^{13} \text{ cm}^{-2}$ for the other positions. Finally, the D_2CO column densities are $\geq 10^{12} \text{ cm}^{-2}$ in all the positions listed in Tab. 2.

Table 3 reports, for each position, the abundance ratios between the deuterated isotopologue and the main species, H_2CO , which are equal to the column densities ratios. Then, following Manigand et al. (2019), the deuterium fractions, D/H, are obtained from the abundance ratios: $\text{D}/\text{H} = 0.5 \times N_{\text{HDCO}}/N_{\text{H}_2\text{CO}}$, and $\text{D}/\text{H} = \sqrt{N_{\text{D}_2\text{CO}}/N_{\text{H}_2\text{CO}}}$.

The D-fraction of H_2CO in the inner envelope of VLA1623 A is 8% for HDCO, and 6% for D_2CO . Remarkably, we report the first estimate of D/H in the cavities opened by the protostellar outflow. Namely, D/H is 6% (HDCO), and 35% (D_2CO) in the SE outflow cavity; and 4% (HDCO), and $\leq 22\%$ (D_2CO) in the NW outflow cavity. Finally, the estimate of D/H in the streamers is not accurate because we only have an upper limit of the excitation temperature, hence a lower limit of the column densities of the three species. However, assuming that H_2CO , HDCO, and D_2CO are excited at the inferred T_{ex} upper limit, we obtain an estimate of the D/H in the streamers: D/H is 3%–15% (for HDCO), and 17% (for D_2CO).

We show the intensity ratio maps of $\text{HDCO}/\text{H}_2\text{CO}$ and $\text{D}_2\text{CO}/\text{H}_2\text{CO}$ in Fig. A6. The maps are integrated taking into account the velocity ranges imaging the V (northern blue-shifted streamer towards A), VII (outflow cavities driven by A), and VII (southern red-shifted streamer towards A) components listed in Table 2 to be consistent with the deuteration derived in the system. The distribution of the ratio maps is consistent with that found in Table 3.

5.2 Comparison with previous results on H_2CO deuteration

Figure 9 compares the D/H values estimated for VLA1623 with previous interferometric measurements obtained for Class 0 hot-corinos and disks either in the context of the FAUST LP (Evans et al. 2023; Podio et al. 2024) or in previous ALMA studies (Persson et al. 2018; Manigand et al. 2020b; van der Marel et al. 2021; Brunken et al. 2022). The range of D/H values found in the envelope, outflow cavities, and infalling streamer of VLA1623 A agrees with earlier findings. Interestingly, both the $[\text{HDCO}]/[\text{H}_2\text{CO}]$ and $[\text{D}_2\text{CO}]/[\text{H}_2\text{CO}]$ abundance ratios in the streamer are in agreement with those found by Podio et al. (2024) in the Class I disk IRS 63. They report a significant increase of the abundance of D_2CO at the location where the infalling streamer collides with the disk, causing a shock and leading to the release in gas-phase of the molecules trapped in the dust mantles. The accretion shock thus reveal the composition of the ices in the disk of IRS 63. However, they cannot determine if the ice composition is inherited from the prestellar stage, or if ices are formed and/or reprocessed in the disk itself. Our observations of VLA1623 shows D_2CO -enriched mantles in the streamer, with D/H ratios similar to those in the Class I disk of IRS 63, thus suggesting that deuteration is mostly set at the prestellar stage, and inherited by the disk at its formation and/or through streamers. The comparison within each class of regions and between types of regions is difficult because of the inherent differences that are already known. These variations can be driven by local physical conditions. Hence the present data call for further observations of other star-forming regions to look for differences in D/H within the same structure (such as along streamers or cavities) which may share similar conditions such as timescale, evolution, and physical conditions.

5.3 On the origin of D_2CO extended emission

ALMA-FAUST interferometric observations show extended emission of D_2CO toward the multiple system VLA1623-2417 for the first time. As reported in Sect. 4, D_2CO emission reveals a puzzling spatial distribution, which does not match that of H_2CO and HDCO. While H_2CO and HDCO emissions have their peak in the hot corino toward VLA1623 A, in the outflow cavities, and in the redshifted southern streamer, D_2CO probes mostly the flattened envelope perpendicular to the outflow direction (see Fig. 1), which is fainter in H_2CO and HDCO. A different spatial distribution of D_2CO with respect to that of H_2CO and HDCO has also been found towards another FAUST protostellar source, the disk-streamer system of IRS 63, and has been interpreted as due to a different chemical origin of D_2CO , with respect to H_2CO and HDCO (Podio et al. 2024).

More specifically, formaldehyde and its deuterated isotopologues can form both in the gas phase and on the surface of dust grains. In warm gas ($\sim 50 \text{ K}$, Parise et al. 2009) H_2CO , HDCO, and D_2CO follow a similar formation path, starting from CH_3^+ which reacts either with H_2 (to form H_2CO), or with HD (to form CH_2D^+ and CHD_2^+ , and from the latter HDCO and D_2CO) (e.g., Roueff et al. 2007, 2013). However, the different spatial distribution of D_2CO points to its formation on the surface of dust grains, following the scheme presented in Fig. 4 by Podio et al. (2024). The processes occurring on the grains may cause an enhancement of the D_2CO abundance with respect to that of HDCO and H_2CO on the ices. Then, when the ice mantles are released in the gas phase due to shocks (as in the case of IRS 63) or to a radiation field, we may observe an enhancement of D_2CO emission, with respect to HDCO and H_2CO .

Following the above reasoning, we propose that in the case of the VLA1623 protostellar cluster, the fact that D_2CO is detected in an extended region where HDCO and H_2CO emission is faint, is due to deuterated molecules formation on the grains in the cold prestellar phase and release in the gas phase due to irradiation within a dense photodissociation region (PDR).

Figure A7 shows the moment 2 (velocity dispersion) map of D_2CO ($4_{0,4} - 3_{0,3}$) emission, which indicates that the extended emission partially traces the outflow cavities and the streamer as listed in Table 2. The extended D_2CO emission shows a narrow velocity dispersion between 0.3 and 1.2 km s^{-1} . This is not consistent with the release of D_2CO molecules in shocks, which would produce large line profiles. Thus, we investigate whether the observed D_2CO emission can be caused by the release of the icy mantles in gas-phase due to a PDR. Rawlings et al. (2013) presented infrared observations taken with WISE (Wide-field Infrared Survey Explorer), *Herschel*, and 2MASS (Two Micron All-Sky Survey), and visual extinction maps towards the VLA1623-2417 region in the Ophiuchus cloud. These maps show that VLA1623-2417 is illuminated by two nearby B stars (HD147889 and ρ Oph AB). Their study suggests high irradiation and an increased emission of PAHs (polycyclic aromatic hydrocarbons). The 2MASS catalog also indicate high visual extinction ($A_V > 30$ mag) towards VLA1623-2417. In addition, polarisation studies with JCMT SCUBA by Pattle et al. (2019) showed evidence of an external radiation field which may cause dust grain alignment.

In summary, the VLA1623-2417 protostellar cluster could be affected by a locally stronger radiation field. Thus, the narrow velocity dispersion of D_2CO emission (Fig. A7) could trace the front of the radiation field caused by the massive B stars and OB association in the Oph A core. If this is the case, D_2CO molecules are photo-desorbed from the grains.

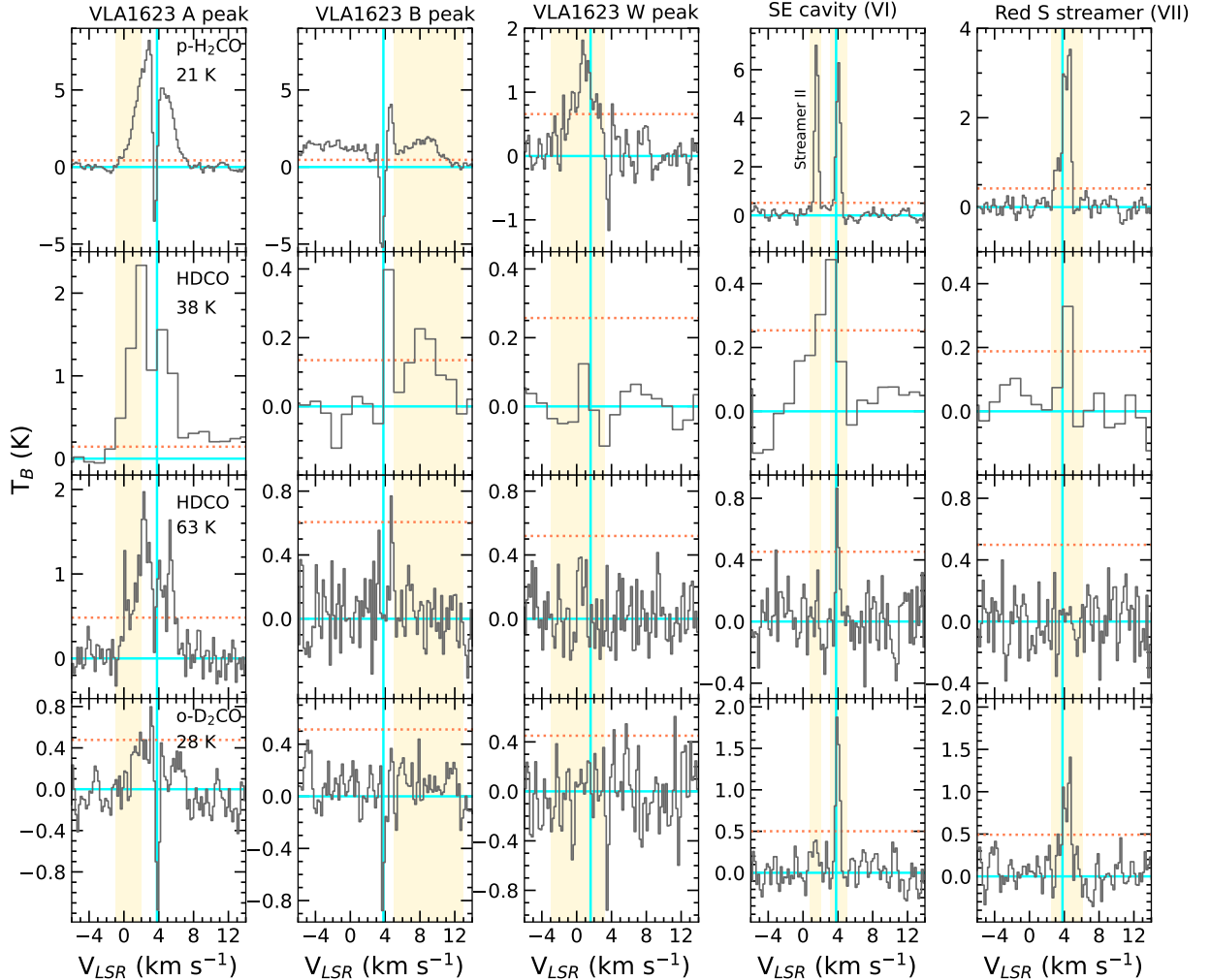


Figure 8. Spectra of the H_2CO , HDCO , and D_2CO lines extracted at several positions of the VLA1623-2417 cluster (in brightness temperature, T_B). Because of the low S/N , for the low-excitation D_2CO ($4_{2,3} - 3_{2,2}$) line we report only the spectrum integrated on a $10''$ region (see Fig. 7). The positions are (from left to right): dust continuum peak of VLA1623 A, B, and W (first, second, and third column, respectively); a position along the SE cavity (VI components, fourth column); a position along the red-shifted southern streamer (VII component, fifth column). The vertical solid line stands for the source systemic velocity ($+3.8 \text{ km s}^{-1}$ for VLA1623 A and B, and $+1.6 \text{ km s}^{-1}$ for VLA1623 W). The orange horizontal dotted line indicates the 3σ level. The blue-shifted emission peak in the H_2CO spectrum of the SE outflow cavity (VI) traces the southern blue-shifted streamer, labeled II in Table 2. Yellow bands show the velocity ranges of integration of the line intensities reported in Table 3.

6 SUMMARY AND CONCLUSIONS

The FAUST ALMA Large Program has imaged deuterated formaldehyde emission in the VLA1623-2417 protostellar cluster down to the spatial scale of 50 au. Emission from H_2CO ($3_{0,3} - 2_{0,2}$), HDCO ($4_{1,4} - 3_{1,3}$), HDCO ($4_{2,2} - 3_{2,1}$), D_2CO ($4_{0,4} - 3_{0,3}$), and D_2CO ($4_{2,3} - 3_{2,2}$) has been detected and shows both extended and compact structures. The main findings are summarised as follows:

(i) The binary system VLA1623 A is associated with formaldehyde and its deuterated isotopologues. Conversely, the VLA1623 B and W protostars have been detected in H_2CO but not in HDCO and

D_2CO . High-velocity formaldehyde emissions trace the two counter-rotating, spatially unresolved cores ($\leq 50 \text{ au}$) of VLA1623 A and VLA1623 B, and the brightest blue-shifted side of the envelope of VLA1623 W;

(ii) H_2CO , HDCO , and D_2CO also probe extended structures, including the symmetric and rotating cavities created by the VLA1623 A outflow, and two extended (approximately 1000 au) accretion streamers feeding the VLA1623 A+B system.

(iii) Based on the ratio of the HDCO lines, we estimate the gas temperature to be approximately 125 K towards the VLA1623 A hot-corino, between 20–40 K in the cavities, and $\leq 15 \text{ K}$ in the streamers;

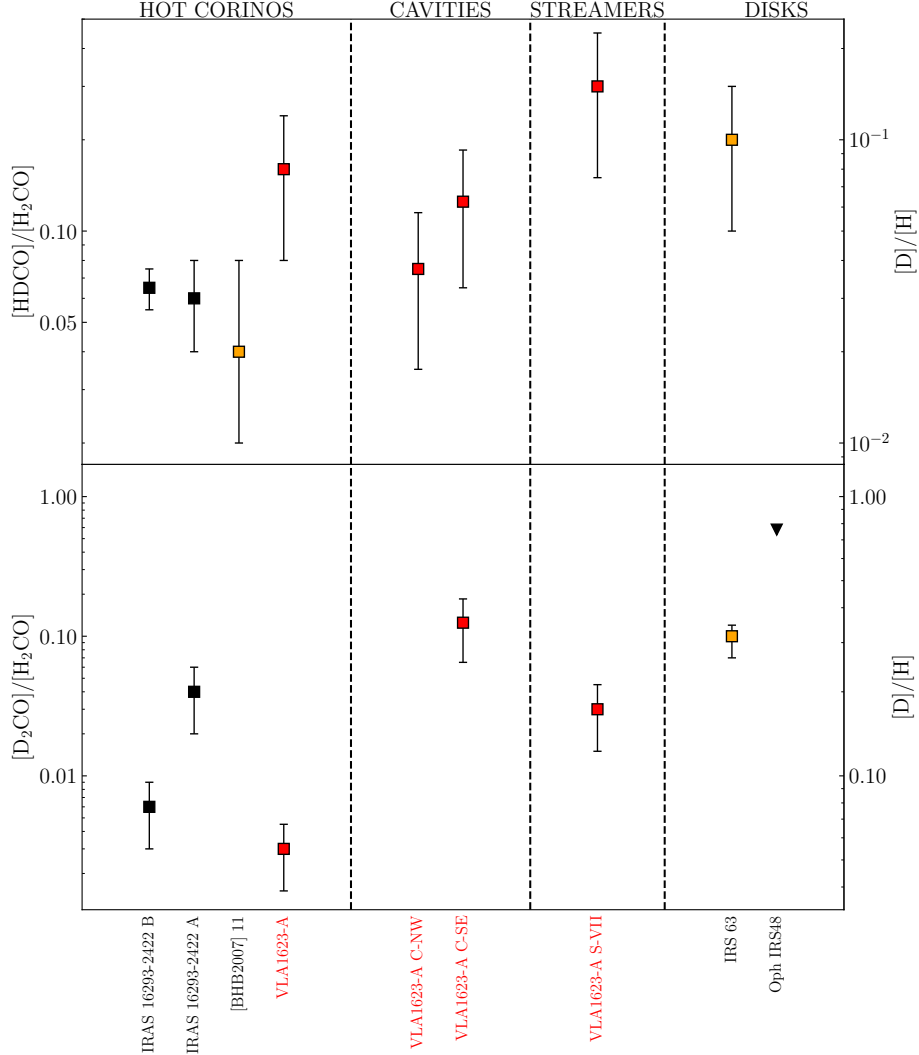


Figure 9. Abundance ratios $[\text{HDCO}]/[\text{H}_2\text{CO}]$ (upper panel), and $[\text{D}_2\text{CO}]/[\text{H}_2\text{CO}]$ (lower panel) estimated through interferometric observations. The abundance ratios (left y-axis) and D/H (right y-axis) derived for VLA1623 hot corino (VLA1623-A), NW and SE outflow cavities (VLA1623-A C-NW and C-SE), and the streamer VII (VLA1623-A S-VII) are indicated by red squares (See Table 3). Previous estimates in Class 0 hot corinos and disks from the literature are reported with black squares (Persson et al. 2018; Manigand et al. 2020a; van der Marel et al. 2021; Brunken et al. 2022), and with orange ones for the ALMA-FAUST studies (Evans et al. 2023; Podio et al. 2024). Upper limits are marked with triangles. The source names are labeled below the bottom panel (in red for the values estimated in this paper for VLA1623). The axes are logarithmic.

(iv) D_2CO reveals an extended component, which is fainter in H_2CO and HDCO, that probes the flattened envelope perpendicular to the outflow direction. We suggest that the extended D_2CO emission results from D_2CO formation on grains during the cold prestellar phase and its release into the gas phase due to the photo-dissociation region caused by two nearby B stars (HD147889 and ρ Oph AB);

(v) The D-fraction of formaldehyde in the hot-corino, outflow cavities, and infalling streamers of VLA1623 A lies in the follow-

ing ranges: $[\text{HDCO}]/[\text{H}_2\text{CO}] \sim 0.07 - 0.3$, and $[\text{D}_2\text{CO}]/[\text{H}_2\text{CO}] \sim 0.003 - 0.13$. These values are comparable to those previously obtained for other Class 0 hot-corinos, as well as for Class I and II disks.

Our results support the hypothesis that deuterated species primarily form during the cold prestellar stage and are subsequently inherited by the forming protostar.

Species	T_{ex} (K)	Velocity range (km s ⁻¹)	Intensity (K km s ⁻¹)	N (cm ⁻²)	[X]/[H ₂ CO]	D/H %
VLA1623 A						
H ₂ CO	125	-1.0 – +2.0	5.9±0.2	3×10^{14}	–	–
HDCO	125(60)	-1.0 – +2.0	6.1±0.2 (38K) / 4.0±0.1 (63K)	$5(3) \times 10^{13}$	0.160	8
D ₂ CO	125	-1.0 – +2.0	0.4±0.1	1×10^{12}	0.003	6
NW Outflow Cavity (VLA1623 B position)						
H ₂ CO	28	+5.0 – +13.0	8.6±0.2	8×10^{13}	–	–
HDCO	28(12)	+5.0 – +13.0	0.9 (38K) / 0.3 (63K)	$6(4) \times 10^{12}$	0.075	4
D ₂ CO	28	+5.0 – +13.0	≤ 0.7±0.1	≤ 4×10^{12}	≤ 0.050	≤ 22
SE Outflow Cavity, VI						
H ₂ CO	37	+3.1 – +5.0	3.7±0.1	4×10^{13}	–	–
HDCO	37(19)	+3.1 – +5.0	0.7 (38K) / 0.3 (63K)	$5(4) \times 10^{12}$	0.125	6
D ₂ CO	37	+3.1 – +5.0	1.1±0.1	5×10^{12}	0.125	35
Streamer II (SE Outflow Cavity position)						
H ₂ CO	≤ 15	+0.8 – +2.1	3.8±0.1	≥ 3×10^{13}	–	–
HDCO	≤ 15	+0.8 – +2.1	0.7±0.1 (38 K)	≥ 2×10^{12}	0.067	3
D ₂ CO	–	–	–	–	–	–
Streamer VII						
H ₂ CO	≤ 10	+2.5 – +6.1	4.1±0.1	≥ 3×10^{13}	–	–
HDCO	≤ 10	+2.5 – +6.1	0.5±0.1 (38 K)	≥ 9×10^{12}	0.300	15
D ₂ CO	≤ 10	+2.5 – +6.1	1.4±0.1	≥ 1×10^{12}	0.030	17

Table 3. Velocity ranges used for line integration (see Fig. 8), integrated line intensities, excitation temperature (T_{ex}), molecular column densities (N), abundance ratios, and D/H ratios towards the protostellar continuum peaks, and selected positions representing the outflow cavities, and the streamers. For HDCO we report the intensity of both lines, indicating their E_{up} (38 K, and 63 K) in parenthesis next to the intensity. The excitation temperature is derived from the ratio of the HDCO lines. For H₂CO and D₂CO, T_{ex} is assumed to be equal to that derived from HDCO. For the streamers, we report the abundance ratios and D/H derived from the lower limits of the column densities.

ACKNOWLEDGEMENTS

We are grateful to the referee P.T.P. Ho for his instructive report. We also thank N. Balucani for precious discussions on the chemistry of formaldehyde isotopologues. This project has received funding from the EC H2020 research and innovation programme for: (i) the project "Astro-Chemical Origins" (ACO, No 811312), and (ii) the European Research Council (ERC) project "The Dawn of Organic Chemistry" (DOC, No 741002). LP, GS, and ClCo acknowledge the PRIN-MUR 2020 BEYOND-2p (Astrochemistry beyond the second period elements, Prot. 2020AFB3FX), the project ASI-Astrobiologia 2023 MIGLIORA (Modeling Chemical Complexity, F83C23000800005), the INAF-GO 2023 fundings PROTO-SKA (Exploiting ALMA data to study planet forming disks: preparing the advent of SKA, C13C23000770005), the INAF Mini-Grant 2022 "Chemical Origins" (PI: L. Podio), and financial support under the National Recovery and Resilience Plan (NRRP), Mission 4, Component 2, Investment 1.1, Call for tender No. 104 published on 2.2.2022 by the Italian Ministry of University and Research (MUR), funded by the European Union – NextGenerationEU– Project Title 2022JC2Y93 Chemical Origins: linking the fossil composition of the Solar System with the chemistry of protoplanetary disks – CUP J53D23001600006 - Grant Assignment Decree No. 962 adopted on 30.06.2023 by the Italian Ministry of University and Research (MUR). G.S. also acknowledges the INAF-Minigrant 2023 TRIESTE ("TRacing the chemical heritage of our origins: from protostars to planets"; PI: G. Sabatini). D.J. is supported by NRC Canada and by an NSERC Discovery Grant. This paper makes use

of the following ALMA data: ADS/JAO.ALMA#2018.1.01205.L. ALMA is a partnership of ESO (representing its member states), NSF (USA), and NINS (Japan), together with NRC (Canada), MOST and ASIAA (Taiwan), and KASI (Republic of Korea), in cooperation with the Republic of Chile. The Joint ALMA Observatory is operated by ESO, AUI/NRAO and NAOJ. The National Radio Astronomy Observatory is a facility of the National Science Foundation operated under a cooperative agreement by Associated Universities, Inc.

DATA AVAILABILITY

The raw data are available on the ALMA archive at the end of the proprietary period (ADS/JAO.ALMA#2018.1.01205.L).

REFERENCES

- Andre P., Martin-Pintado J., Despois D., Montmerle T., 1990, *A&A*, **236**, 180
 Bacmann A., Lefloch B., Ceccarelli C., Castets A., Steinacker J., Loinard L., 2002, *A&A*, **389**, L6
 Bacmann A., Lefloch B., Ceccarelli C., Steinacker J., Castets A., Loinard L., 2003, *ApJ*, **585**, L55
 Bianchi E., et al., 2017, *MNRAS*, **467**, 3011
 Brunken N. G. C., Booth A. S., Leemker M., Nazari P., van der Marel N., van Dishoeck E. F., 2022, *A&A*, **659**, A29
 CASA Team et al., 2022, *PASP*, **134**, 114501

- Caselli P., Ceccarelli C., 2012, *A&ARv*, 20, 56
- Caselli P., Walmsley C. M., Tafalla M., Dore L., Myers P. C., 1999, *ApJ*, 523, L165
- Caselli P., Walmsley C. M., Zucconi A., Tafalla M., Dore L., Myers P. C., 2002, *ApJ*, 565, 344
- Ceccarelli C., Caselli P., Herbst E., Tielens A. G. G. M., Caux E., 2007, in Reipurth B., Jewitt D., Keil K., eds, *Protostars and Planets V*. p. 47 ([arXiv:astro-ph/0603018](https://arxiv.org/abs/astro-ph/0603018))
- Ceccarelli C., Caselli P., Bockelée-Morvan D., Mousis O., Pizzarello S., Robert F., Semenov D., 2014, in Beuther H., Klessen R. S., Dullemond C. P., Henning T., eds, *Protostars and Planets VI*. pp 859–882 ([arXiv:1403.7143](https://arxiv.org/abs/1403.7143)), doi:10.2458/azu_uapress_9780816531240-ch037
- Ceccarelli C., et al., 2023, in Inutsuka S., Aikawa Y., Muto T., Tomida K., Tamura M., eds, *Astronomical Society of the Pacific Conference Series Vol. 534*, Astronomical Society of the Pacific Conference Series. p. 379
- Chacón-Tanarro A., et al., 2019, *A&A*, 622, A141
- Chahine L., et al., 2024, *MNRAS*, 534, L48
- Codella C., Ceccarelli C., Chandler C., Sakai N., Yamamoto S., FAUST Team 2021, *Frontiers in Astronomy and Space Sciences*, 8, 227
- Codella C., et al., 2022, *MNRAS*, 515, 543
- Codella C., et al., 2024, *arXiv e-prints*, p. [arXiv:2402.10258](https://arxiv.org/abs/2402.10258)
- Cooke R. J., Pettini M., Steidel C. C., 2018, *ApJ*, 855, 102
- Crapsi A., Caselli P., Walmsley C. M., Myers P. C., Tafalla M., Lee C. W., Bourke T. L., 2005, *ApJ*, 619, 379
- Drozdovskaya M. N., et al., 2021, *MNRAS*, 500, 4901
- Emprechtinger M., Caselli P., Volgenau N. H., Stutzki J., Wiedner M. C., 2009, *A&A*, 493, 89
- Evans L., et al., 2023, *A&A*, 678, A160
- Fuchs G. W., Cuppen H. M., Ioppolo S., Romanzin C., Bisschop S. E., Andersson S., van Dishoeck E. F., Linnartz H., 2009, *A&A*, 505, 629
- Gagné J., et al., 2018, *ApJ*, 856, 23
- Garrod R. T., Jin M., Matis K. A., Jones D., Willis E. R., Herbst E., 2022, *ApJS*, 259, 1
- Gerlich D., Herbst E., Roueff E., 2002, *Planet. Space Sci.*, 50, 1275
- Hara C., et al., 2021, *ApJ*, 912, 34
- Harris R. J., et al., 2018, *ApJ*, 861, 91
- Hsieh C.-H., Lai S.-P., Cheong P.-I., Ko C.-L., Li Z.-Y., Murillo N. M., 2020, *ApJ*, 894, 23
- Loinard L., Castets A., Ceccarelli C., Caux E., Tielens A. G. G. M., 2001, *ApJ*, 552, L163
- Looney L. W., Mundy L. G., Welch W. J., 2000, *ApJ*, 529, 477
- Manigand S., et al., 2019, *A&A*, 623, A69
- Manigand S., et al., 2020a, *A&A*, 635, A48
- Manigand S., et al., 2020b, *A&A*, 635, A48
- Mercimek S., et al., 2022, *A&A*, 659, A67
- Mercimek S., et al., 2023, *MNRAS*, 522, 2384
- Müller H. S. P., Schlöder F., Stutzki J., Winnewisser G., 2005, *Journal of Molecular Structure*, 742, 215
- Murillo N. M., Lai S.-P., Bruderer S., Harsono D., van Dishoeck E. F., 2013, *A&A*, 560, A103
- Murillo N. M., Harsono D., McClure M., Lai S. P., Hogerheijde M. R., 2018a, *A&A*, 615, L14
- Murillo N. M., van Dishoeck E. F., van der Wiel M. H. D., Jørgensen J. K., Drozdovskaya M. N., Calcutt H., Harsono D., 2018b, *A&A*, 617, A120
- Ohashi S., et al., 2022, *ApJ*, 927, 54
- Parise B., Ceccarelli C., Tielens A. G. G. M., Castets A., Caux E., Lefloch B., Maret S., 2006, *A&A*, 453, 949
- Parise B., Leurini S., Schilke P., Roueff E., Thorwirth S., Lis D. C., 2009, *A&A*, 508, 737
- Pattle K., et al., 2019, *ApJ*, 880, 27
- Persson M. V., et al., 2018, *A&A*, 610, A54
- Podio L., et al., 2024, *arXiv e-prints*, p. [arXiv:2407.04813](https://arxiv.org/abs/2407.04813)
- Rawlings M. G., Juvela M., Lehtinen K., Mattila K., Lemke D., 2013, *MNRAS*, 428, 2617
- Roberts H., Millar T. J., 2000, *A&A*, 364, 780
- Roueff E., Herbst E., Lis D. C., Phillips T. G., 2007, *ApJ*, 661, L159
- Roueff E., Gerin M., Lis D. C., Wootten A., Marcelino N., Cernicharo J., Tercero B., 2013, *Journal of Physical Chemistry A*, 117, 9959
- Sabatini G., et al., 2020, *A&A*, 644, A34
- Sabatini G., et al., 2022, *ApJ*, 936, 80
- Sabatini G., et al., 2024, *A&A*, 684, L12
- Sakai N., et al., 2014a, *Nature*, 507, 78
- Sakai N., et al., 2014b, *ApJ*, 791, L38
- Santangelo G., Murillo N. M., Nisini B., Codella C., Bruderer S., Lai S. P., van Dishoeck E. F., 2015, *A&A*, 581, A91
- Taquet V., et al., 2019, *A&A*, 632, A19
- Tielens A. G. G. M., 1983, *A&A*, 119, 177
- Turner B. E., 2001, *ApJS*, 136, 579
- Vastel C., Phillips T. G., Yoshida H., 2004, *ApJ*, 606, L127
- Ward-Thompson D., Kirk J. M., Greaves J. S., André P., 2011, *MNRAS*, 415, 2812
- van der Marel N., Booth A. S., Leemker M., van Dishoeck E. F., Ohashi S., 2021, *A&A*, 651, L5

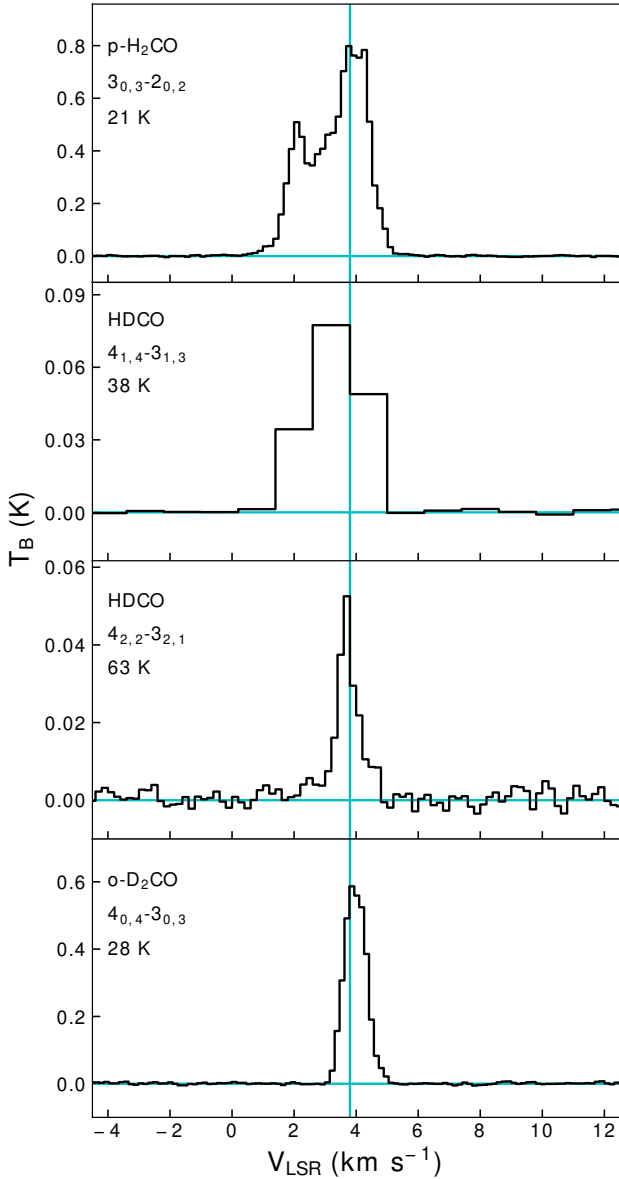


Figure A1. Spectra (in brightness temperature, T_B , scale) observed towards VLA1623 and obtained integrating the emission over the FoV (see Table 1). From top to bottom: H_2CO ($3_{0,3} - 2_{0,2}$), HDCO ($4_{2,2} - 3_{2,1}$), HDCO ($4_{2,2} - 3_{2,1}$), and D_2CO ($4_{0,4} - 3_{0,3}$). The cyan vertical line represents the systemic velocity of VLA1623 A and B: $+3.8 \text{ km s}^{-1}$ (Ohashi et al. 2022).

APPENDIX A: ADDITIONAL MATERIAL

A1 Integrated spectra towards VLA1623–2417

Figure A1 reports the spectra (in brightness temperature, T_B , scale) obtained integrating the line emission over the FoV of the VLA1623–2417 observations (see Table 1).

A2 Channel maps of the HDCO lines

We report the channel maps of the HDCO $4_{1,4} - 3_{1,3}$ (Fig. A2), and $4_{2,2} - 3_{2,1}$ (Fig. A3) emission. We show both high-velocity emission on small spatial scale (upper panels), and low-velocity emission on large spatial scales (lower panels).

A3 Integrated intensity (moment 0) maps of D_2CO ($4_{0,4} - 3_{0,3}$)

We present the integrated intensity maps (moment 0) of D_2CO ($4_{0,4} - 3_{0,3}$) towards VLA1623–2417 integrated on different velocity ranges in Fig. A4.

A4 Channel maps of the D_2CO ($4_{2,3} - 3_{2,2}$)

Figure A5 shows the channel maps of the D_2CO ($4_{2,3} - 3_{2,2}$) emission in VLA1623–2417.

A5 Intensity ratio maps of $\text{HDCO}/\text{H}_2\text{CO}$ and $\text{D}_2\text{CO}/\text{H}_2\text{CO}$

Figure A6 shows the Intensity ratio maps of $\text{HDCO}(4_{1,4} - 3_{1,3})/\text{p-H}_2\text{CO}(3_{0,3} - 2_{0,2})$ (upper rows) and $\text{o-D}_2\text{CO}(4_{0,4} - 3_{0,3})/\text{p-H}_2\text{CO}(3_{0,3} - 2_{0,2})$ (bottom rows) towards the VLA1623–2417. region. In particular, three components are imaged: (see Tab. 2): northern blue-shifted streamer towards A (label V), outflow cavities driven by A (VI), and southern red-shifted streamer towards A (VII).

A6 Intensity-weighted mean velocity and velocity-dispersion maps of D_2CO ($4_{0,4} - 3_{0,3}$)

We present the intensity-weighted mean velocity (moment 1) and velocity–dispersion (moment 2) maps of D_2CO ($4_{0,4} - 3_{0,3}$) emission spanning the velocity range from $+3.0 \text{ km s}^{-1}$ to $+5.2 \text{ km s}^{-1}$ towards VLA1623–2417 in Fig. A7

This paper has been typeset from a $\text{\TeX}/\text{\LaTeX}$ file prepared by the author.

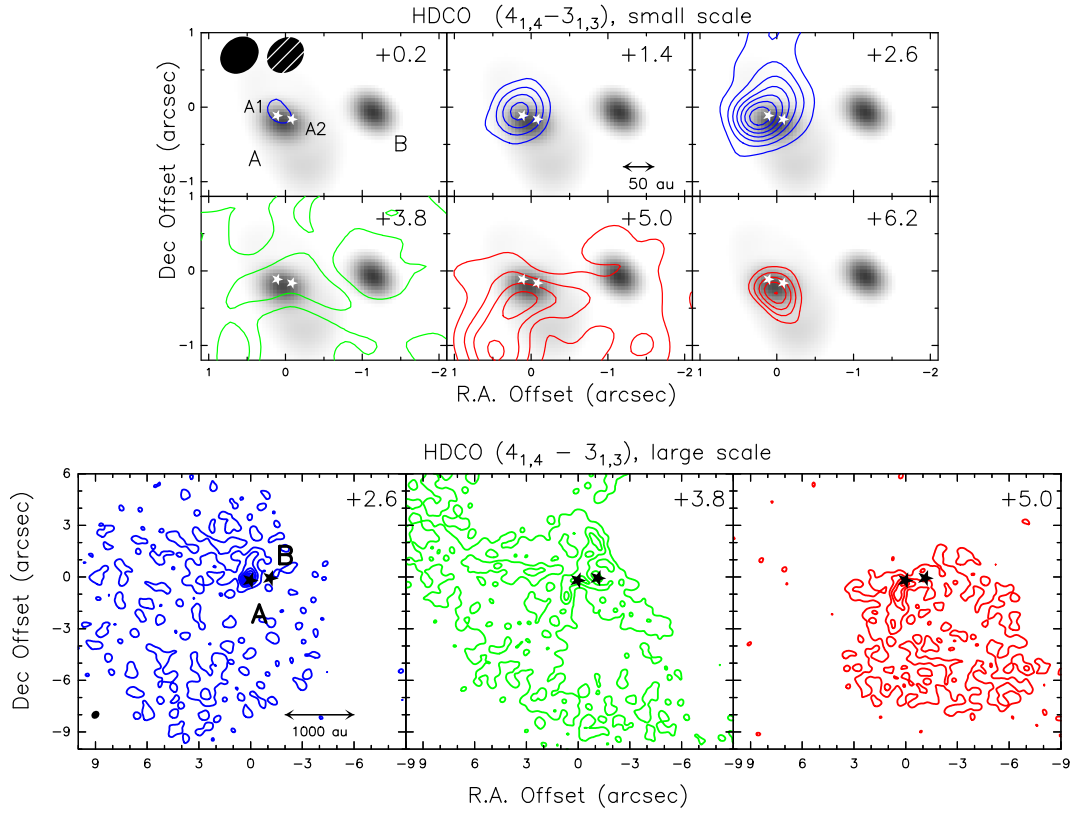


Figure A2. *Top:* Channel maps of HDCO $4_{1,4} - 3_{1,3}$ emission at small scale. The first contour and step is at 3σ ($2.1 \text{ mJy beam}^{-1}$). The grayscale background shows the 1.3 mm continuum emission in Setup 2. The synthesized beams are shown in the top-left corner of the first channel by filled and dashed ellipses for line and continuum emission, respectively. White stars indicate the positions of VLA1623 A1 and A2 from (Harris et al. 2018). VLA 1623 A1, A2, A, and B are labeled in the first channel. *Bottom:* Channel maps of HDCO $4_{1,4} - 3_{1,3}$ emission at large scale, in the velocity range between $+2.6 \text{ km s}^{-1}$ and $+5.0 \text{ km s}^{-1}$. The black stars indicate VLA1623 A and VLA1623 B as detected in the FAUST continuum maps at 1.3 mm.

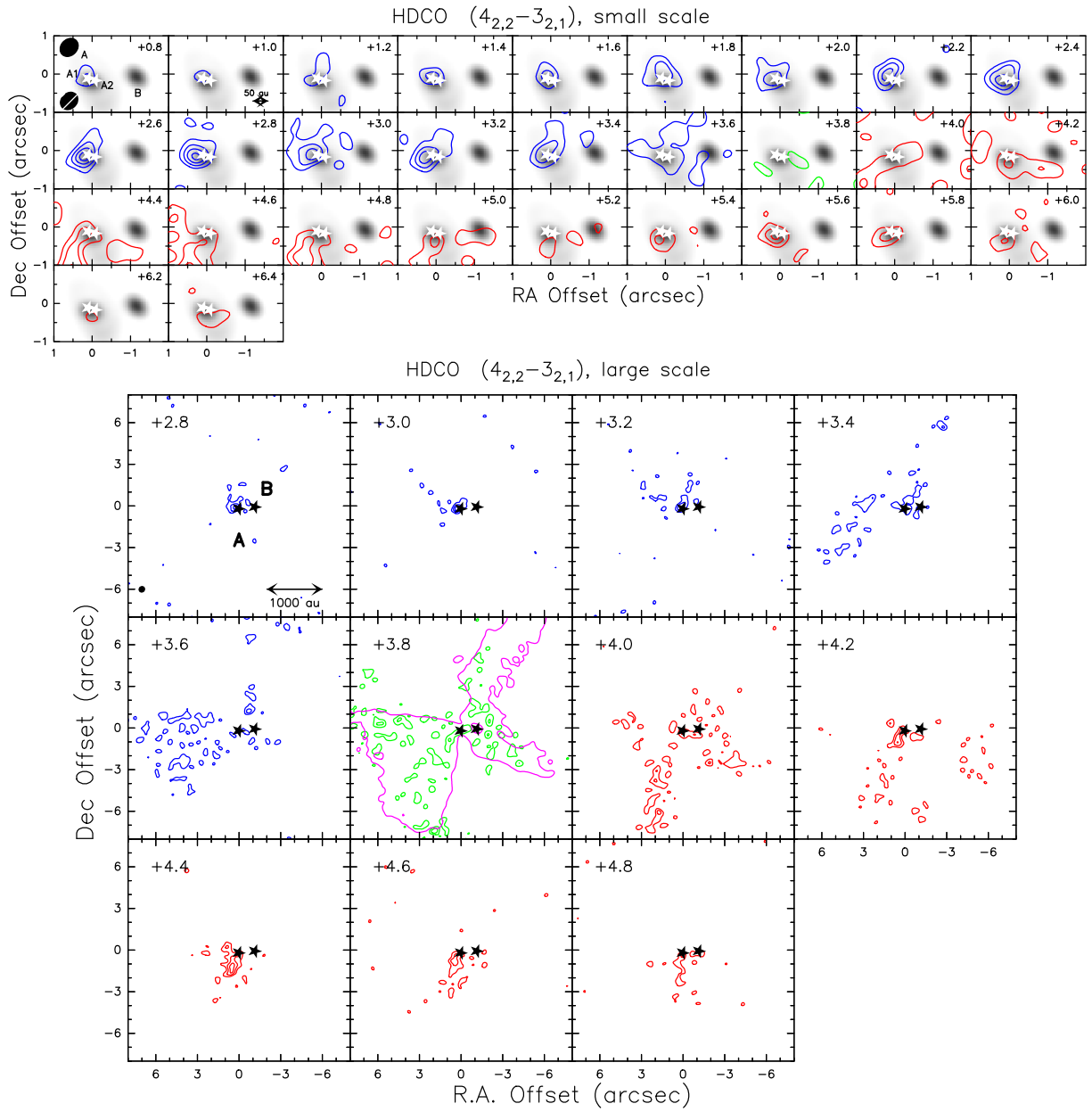


Figure A3. *Top:* Channel maps of HDCO $4_{2,2} - 3_{2,1}$ at small scale. The first contour and step is at 6σ ($2.0 \text{ mJy beam}^{-1}$). The grayscale background shows the 1.3 mm continuum emission in Setup 2. The synthesized beams are shown in the left corner of the first channel by filled and dashed ellipses for line and continuum emission, respectively. White stars indicate the positions of VLA1623 A1 and A2 from (Harris et al. 2018). VLA1623 A1, A2, A, and B are labeled in the first channel. *Bottom:* Channel maps of HDCO $4_{1,4} - 3_{1,3}$ at large scale, in the velocity range ($[+2.8, +4.8] \text{ km s}^{-1}$). The black stars indicate VLA1623 A and VLA1623 B as detected in the FAUST continuum map at 1.3 mm. The magenta contour in the channel at $+3.8 \text{ km s}^{-1}$ indicates the outflow cavity walls probed by CS (5-4) (25σ contour, from Ohashi et al. 2022).

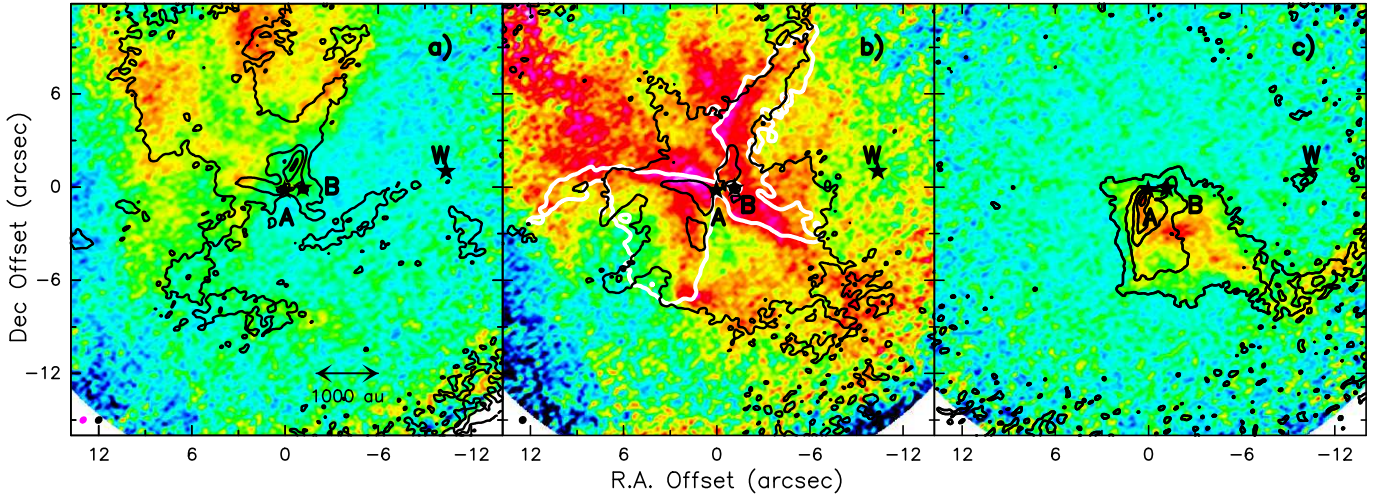


Figure A4. Integrated intensity (moment 0) maps of D_2CO ($4_{0,4} - 3_{0,3}$) emission (color) and H_2CO ($3_{0,3} - 2_{0,2}$) emission in black contours. The emission structures identified in the H_2CO and D_2CO emission in Panels a), b), and c) are labeled as V, VI, VII and are integrated on the velocity ranges listed in Table 2. The first contour is at 3σ , and the step is 6σ : for Panel a) σ is $2.2 \text{ mJy km s}^{-1} \text{ beam}^{-1}$, for Panel b) σ is $12.0 \text{ mJy km s}^{-1} \text{ beam}^{-1}$, for Panel c) σ is $4.5 \text{ mJy km s}^{-1} \text{ beam}^{-1}$. White contour in panel b) indicates the outflow cavity walls probed by CS ($5-4$) (25σ contour, from Ohashi et al. 2022). The synthesized beams are shown by the magenta and black ellipses in the bottom-left corner of the panel a) for the D_2CO and H_2CO , respectively, and by the black ellipse in the bottom-left corner of the panel b) for CS. The positions of VLA1623 A, B, and W are indicated by the black stars and are labeled.

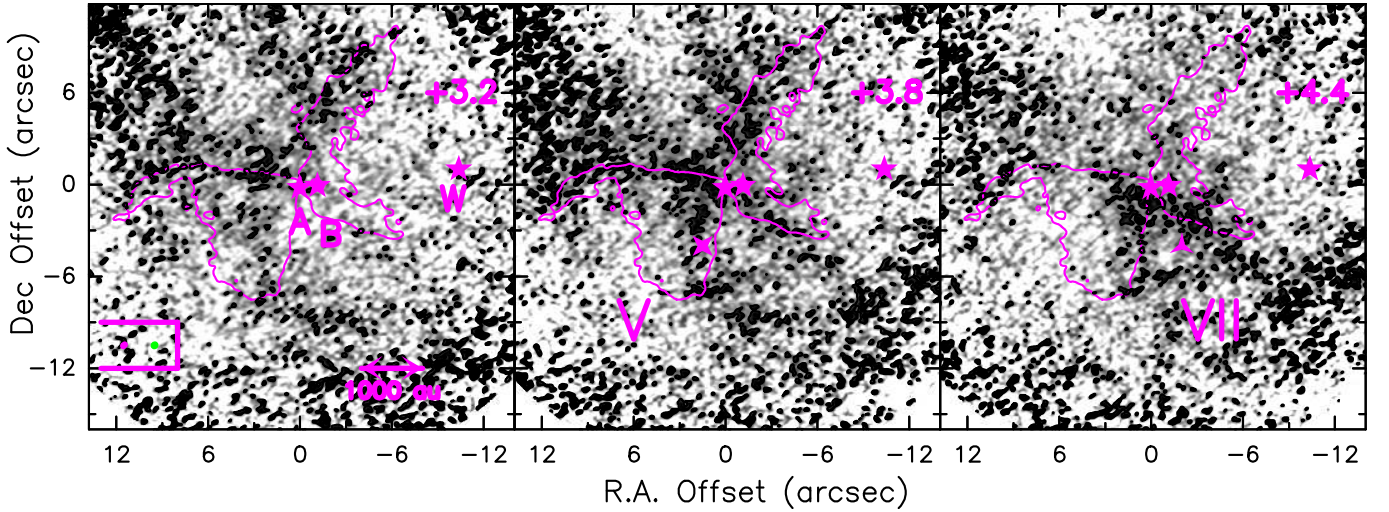


Figure A5. Channel maps of the D_2CO ($4_{2,3} - 3_{2,2}$) emission in the velocity range $[+3.2, +4.4] \text{ km s}^{-1}$. The first contour is at 3σ , and the step is 3σ . The magenta contours indicate the outflow cavity walls probed by CS ($5-4$) (25σ contour, from Ohashi et al. 2022). The magenta and green ellipses in the bottom-left corner of the first channel show the synthesized beams for the CS ($5-4$) and D_2CO emission, respectively. The positions of VLA1623 A, B, and W are indicated by the magenta stars and are labeled in the first channel. The large-scale emissions are labeled as "VI" and "VII" in Table 2 consistently with the H_2CO components. Magenta cross and triangle symbols in the channels between $+3.8$ and $+4.4 \text{ km s}^{-1}$ show the position along the outflow cavity wall and the streamer where the spectra are extracted (Fig. 8 in Sect. 5.1).

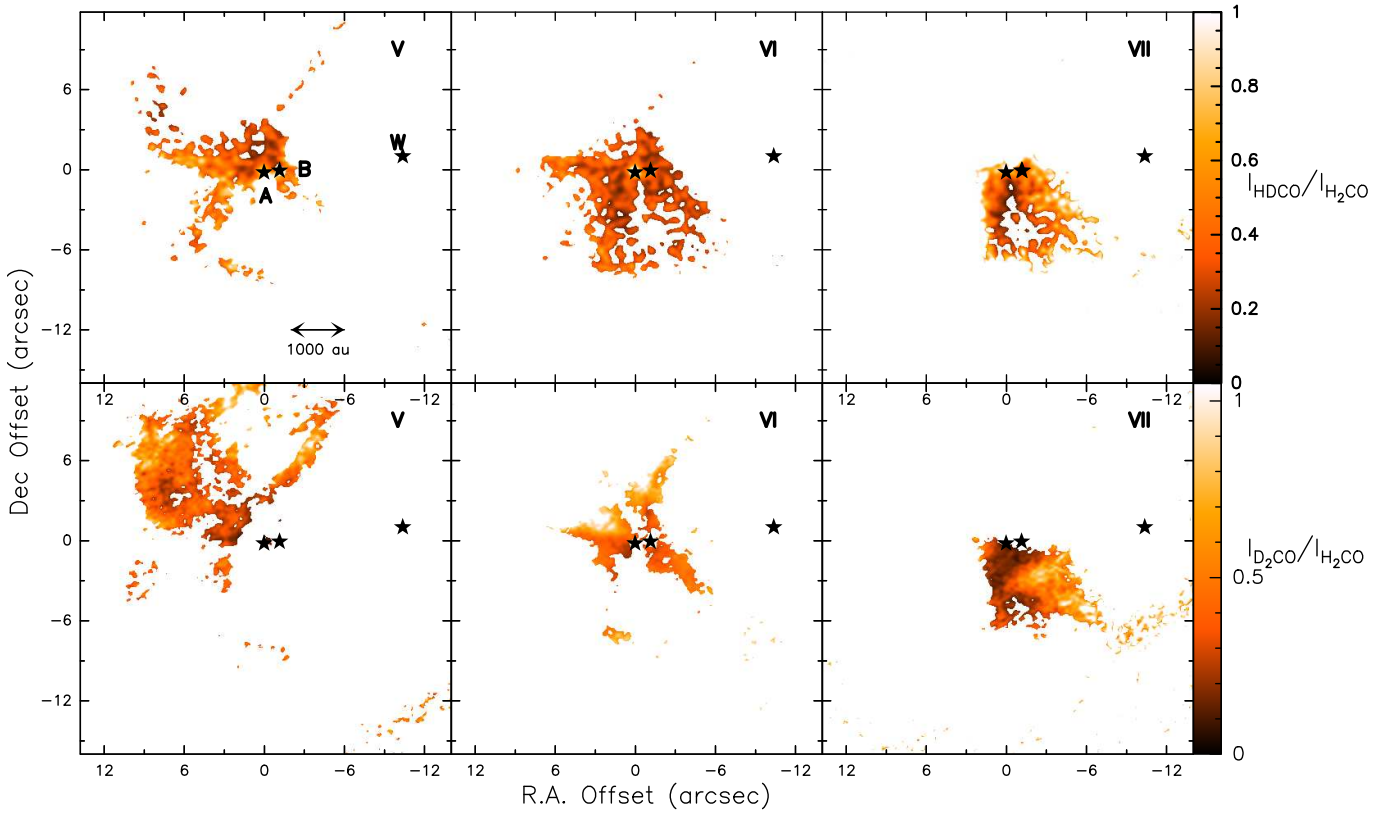


Figure A6. Intensity ratio maps of $\text{HDCO}(4_{1,4} - 3_{1,3})/p\text{-H}_2\text{CO}(3_{0,3} - 2_{0,2})$ (upper rows) and $o\text{-D}_2\text{CO}(4_{0,4} - 3_{0,3})/p\text{-H}_2\text{CO}(3_{0,3} - 2_{0,2})$ (bottom rows) for three components of the VLA1623-2417 region (see Tab. 2): northern blue-shifted streamer towards A (label V), outflow cavities driven by A (VI), and southern red-shifted streamer towards A (VII). The color bars are shown at the right corners related to the ratio molecules. The positions of VLA1623 A, B, and W are indicated by the black stars, and labeled in the first panel.

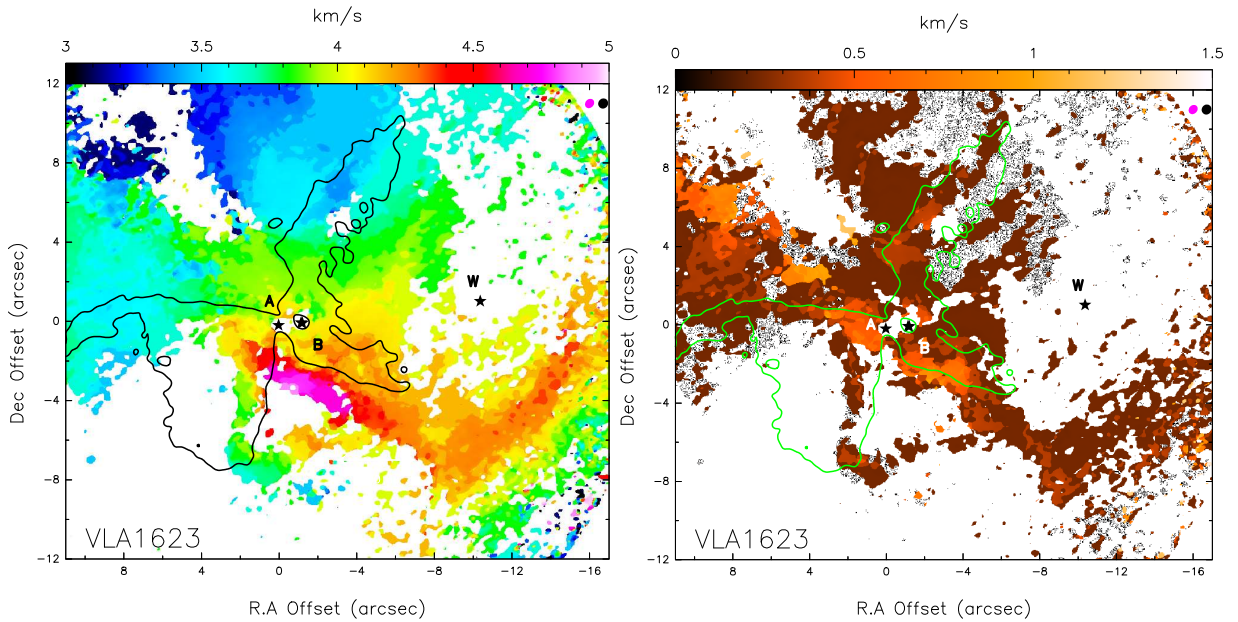


Figure A7. *Left:* Intensity-weighted mean velocity (moment 1) map of $\text{D}_2\text{CO}(4_{0,4} - 3_{0,3})$ emission towards VLA1623-2417 over the velocity range between $+3.0 \text{ km s}^{-1}$ and $+5.2 \text{ km s}^{-1}$. The black contour indicates the outflow cavity walls probed by CS(5-4) (25σ contour, from Ohashi et al. 2022). The synthesized beams are shown by the magenta and black ellipses in the top-right corner for the D_2CO and CS(5-4) emission, respectively (see Tab. 1). *Right:* Velocity-dispersion (moment 2) map of $\text{D}_2\text{CO}(4_{0,4} - 3_{0,3})$ towards VLA1623-2417 over the velocity range between $+3.0 \text{ km s}^{-1}$ and $+5.2 \text{ km s}^{-1}$. The green contour indicates the outflow cavity walls probed by CS(5-4). The positions of VLA1623 A, B, and W are indicated by the black stars, and labeled in the first panel.